ROTATION AND MASSES OF GALAXIES AS DETERMINED BY SINGLE SPACING INTERFEROMETRY OF 21 CM HYDROGEN EMISSION

by

David Herbert Rogstad

In Partial Fulfillment of the Requirements

For the Degree of

Doctor of Philosophy

California Institute of Technology

Pasadena, California

1967

(Submitted October 10, 1966)

Abstract

A total of 79 galaxies have been investigated with the Owens Valley Observatory's two-element interferometer for content of neutral hydrogen. The baseline used was 100 feet east-west, and the filter bandwidth was 100 kHz. Thirty of the galaxies had detectable emission ($>$ 0.5 f.u.). The results are presented as line and position profiles for each galaxy (i.e. plots of the flux, and its position derived from the interferometer phase as a function of radial velocity).

An extensive investigation of model profiles is also presented for the purposes of interpretation of the observed results. It is shown that while in most cases the position profile cannot be directly interpreted as the rotation curve, the model analysis does suggest a method for estimating the rotational characteristics of the galaxies from the profiles.

Using the estimated rotational parameters, total masses were calculated and are presented along with other quantities derivable from the profiles, such as the galaxy radial velocities and estimates of the neutral hydrogen masses.

All of the irregular galaxies that were detected were found to be rotating, with the exception of WLM, which was inconclusive.

Acknowledgements

I wish to gratefully acknowledge J. B. Whiteoak for the tremendous amount of work he did to start this project, and for his encouragement and help along the way.

My deepest appreciation goes to M. Schmidt for his many helpful discussions, encouragement when things looked dark, and critical reading of the manuscript.

Thanks are due to G. W. Rougoor for help with the observations and reductions, to G. A. Seielstad for reading the manuscript and giving many helpful hints on its organization, and to all the Observatory staff for providing an enjoyable and fruitful observation run.

I wish to thank the Observatory director, G. J. Stanley, for his enthusiasm for the project, and for the telescope and computer time to complete it.

And last, but not least, I wish to thank two of my fellow graduate students, E. B. Fomalont and J. F. Bartlett for their generous help with the computer, and for making the life of a grad student a little more human.

I dedicate this thesis to the little fellow who was supposed to wait until its completion before being born, my son Timothy David Rogstad.

Table of Contents

I. Introduction

Since the work of Babcock (1939) on M31, a considerable number of investigations have been devoted to the determination of the rotational characteristics of galaxies. These were spurred on by the fact that direct estimates of some important parameters, such as the mass density and total mass of the galaxy, can be made from knowledge of these characteristics. While some difficulty has been encountered in determining the relationship between the rotation curve and the mass density of a galaxy, the most serious problem has been the measurement of this curve.

Techniques for measuring the rotation curve have been basically of two types: (1) optical spectroscopic observations of various emission lines from HII regions, or lines due to stellar absorption, and (2) radio astronomical observations of the 21 cm line of neutral hydrogen. Until a few years ago the first method was used exclusively, but has been complemented in the past ten years by the second. The optical technique has the advantage of high spatial resolution, a property not yet achieved in a practical sense in radio observations. The largest radio antenna used so far is 300 feet in diameter, giving a resolution of about 10' of arc or a measurement

of position in the sky with errors on the order of 2' of arc, and therefore meaningful results only for galaxies of large apparent size. On the other hand, the 21 cm line has very narrow natural line width, and for many galaxies is very intense. This allows, in contrast to optical work, where for the cases of interest the line intensity is low, high spectral resolution and accurate measurement of velocity. It is also felt that the HI regions in the galaxies probably have a velocity more representative of the general motion of the galaxy, while the HII regions, because of their smaller size, may have their own peculiar velocity and therefore a large dispersion in velocity around the general motion. It is clear that the true rotational characteristics of galaxies will be determined best by combining both of these methods.

In an attempt to obtain better spatial resolution for the hydrogen line method, the technique used for the present observations took advantage of the resolution effects that could be obtained with a single-spacing interferometer to measure accurate positions in the sky. It allowed the position of the centroid of hydrogen emission associated with a given velocity interval to be determined accurately and presented as a "position profile", i.e. a plot of sky position versus velocity. If the galaxy rotates as a solid body in the region that contains

detectable quantities of neutral hydrogen, then the position profile is the rotation curve for this region of the galaxy. Seielstad and Whiteoak (1965), in a preliminary survey of a few galaxies, assumed this was the case, and their results seemed to substantiate this assumption. However, subsequent model analysis and observations of more galaxies have suggested that the assumption is probably not true for most actual cases. The apparent agreement of observation and assumption in the preliminary survey can be accounted for by resolution effects of the interferometer.

The model analysis, however, does suggest a method for interpreting the type of rotation present in a galaxy, and estimating the rotational parameters of a model for each type. Therefore the use of a single spacing interferometer for determining rotation in galaxies still appears to be a valuable technique.

This thesis is divided into two sections. The first discusses the observations of the 21 cm radiation, both line and continuum, from galaxies, and their interpretation. Further work is suggested. The second section covers the brief set of observations of hydrogen line and continuum radiation in clusters of galaxies. Possible future observations are also discussed here.

The observations described were performed jointly with J. B. Whiteoak and G. W. Rougoor, using the

Owens Valley Radio Observatory's twin-element interferometer.

II. Observations of Galaxies

A. Previous Related Work

The history of investigations of neutral hydrogen by radio observations of the 21 cm hyperfine line extends back only a few years to the discovery of the line by Ewen and Purcell (1951). Since this initial work in 1951, hydrogen line investigations have accounted for a large part of the efforts in radio astronomy. Numerous studies of both our own galaxy and other extra-galactic objects have been performed, using the hydrogen line to determine both their structure and rotational characteristics. The advantages of the 21 cm line for these types of observations are manifold, a few being: high transparency of the interstellar material to decimeter radiation; a high intensity line from the large quantities of hydrogen present in many galaxies; and narrow natural linewidth which implies that broadening can usually be associated with the Doppler effect from motion of the atoms.

The most extensive observations of our galaxy have been done at Leiden Observatory in Holland (cf. Muller and Westerhout (1957), Westerhout (1957), Schmidt (1957), van Woerden, Takakubo and Braes (1962), and Rougoor (1964)), and at the CSIRO in Sydney, Australia (cf. Kerr, Hindman

and Gum (1959)). A combined map of the neutral hydrogen concentration was published by Oort, Kerr and Westerhout (1958), which suggested strongly the presence of spiral structure in the Galaxy. These investigations also included a derived rotation curve of the Galaxy.

The first observations of extragalactic neutral hydrogen were done by Kerr, Hindman, and Robinson (1954), when they studied the Magellanic Clouds. Kerr and de Vaucouleurs (1955), in a paper interpreting these results, published temperature contour maps and rotation curves for both the Small and Large Clouds derived from the line profiles. The fruitfulness of this work spurred on further investigations by van de Hulst, Raimond, and van Woerden (1957), Volders (1959), Volders and Högbom (1961), Heidmann (1961), Dieter (1962 a,b,c), and Argyle (1965). These efforts included extensive observations of M31, M33, M51, and M82, but were limited by the resolution of the telescopes used. Roberts (1962) and Epstein (1964) have done observations on many more galaxies, but again with limited resolution. Since then more detailed observations of M31 have been done by Burke (1963) and Roberts (1966a), and of many other galaxies by Roberts (1966b), using the higher resolving power of the 300-foot transit dish at the N.R.A.O.

One of the principal aims of many of these

investigations has been to determine the rotation curves of the galaxies observed, and from these to derive estimates of their masses. The method of using the hydrogen line for determination of the rotation curve has proved to be very effective for the nearer, large galaxies, but is still seriously limited by the lack of resolution for the galaxies of smaller apparent size.

Optical spectroscopic observations of emission and absorption lines from galaxies have also been used to derive rotation curves. Babcock (1939) observed mainly H and K stellar absorption lines in the central regions of M31, and the H_β emission line from several HII regions in its outer extremities. By relating the frequency shift of the various lines to the Doppler velocities of the regions of the galaxy where the lines originated, he obtained a rotation curve for this galaxy. Mayall and Aller (1942) continued this work, using many more emission nebula. Extensive work on other galaxies using primarily the H_α line from HII regions has been carried out by the Burbidges in conjunction with Rubin, Crampton, and Prendergast in a series of papers beginning with Burbidge, Burbidge and Prendergast (1959), the last one being Rubin, Burbidge, Burbidge, Crampton, and Prendergast (1965).

The results of all of the above work that is of interest here can be briefly summarized as follows:

(i) The neutral hydrogen in spiral galaxies is confined to a thin disc, and can be considered more or less constant in density over their extent, dropping to a low value rather quickly at the outer extremities and perhaps having a lower value near the central regions. High resolution studies of the Galaxy and M31 suggest the existence of a ring structure in the hydrogen concentration about half way out in the galaxy where the density is two or three times greater than the surrounding region.

(ii) The rotation curves of the spirals all show a solid body rotation curve near their central regions, except perhaps the Galaxy, where it is not too well known. Many of the observed curves reach a maximum in velocity, and turn over into a tail of decreasing velocity as a function of radius. This has been most evident in optical work. Some of the rotation curves suggest a fairly constant velocity variation with radius.

(iii) The observations of the irregular galaxies indicate rotation in some, but little is known of their rotational parameters. The Magellanic Clouds are the only irregulars for which the rotation curves are known well, and they are very similar to the curves observed in spirals.

A preliminary investigation of neutral hydro-

gen in galaxies using an interferometer was begun by Seielstad and Whiteoak (1965) to test the possibility of using its properties for measuring rotation curves. The present observations continue this work both in the number of galaxies observed, and the interpretation of the information that is obtained with the interferometer.

B. Observing Program

Selection of a list of galaxies for observation was based primarily on two criteria: (1) the size of the galaxy, and (2) the distance of the galaxy. It was considered desirable for ease of observation and interpretation to have as large a portion of the galaxy as possible contained within the primary beam of the antennas (32' of arc beamwidth). Therefore the "optical size" of the galaxies was limited to 32' of arc. The optical dimensions were obtained from de Vaucouleur's Catalogue (1964) and from Epstein (1964). The term is defined in Section E. The restriction placed on the distance of the galaxy was to pick the closer candidates to increase the probability of detecting hydrogen line radiation. The redshift was limited to less than 2500 km/sec. Some galaxies were rejected because of lack of time in the observing schedule. Basically an attempt was made to pick all nearby galaxies that were large, but less than

32' of arc in size, and as many different types as possible.

The Humason, Mayall, and Sandage Catalogue (1956), de Vaucouleur's Catalogue (1964), and lists of hydrogen-containing galaxies such as found in Epstein (1964) served as sources of possible candidates for observation. A list of 74 galaxies was finally selected and observed. It is found in Table 1. One galaxy was included from the preliminary survey (Seielstad and Whiteoak 1965) for cross-checking and error analysis.

Table 1 contains, along with the galaxy name, the galaxy type and notes indicating whether or not hydrogen and/or continuum radiation was detected.

Instabilities in the phase and gain of the interferometer over the course of a day required the calibration of these parameters about once every hour. This was accomplished by means of standard source observations at intervals over the day. An accurate position and flux was available for these standards. They were chosen to be unresolved by the interferometer at the spacing used. Table 2 gives a list of these calibrator sources together with their positions (epoch 1950) and fluxes. The positions given were taken from a list prepared by Fomalont (1966). The fluxes were determined during the course of the observations.

TABLE 1 OBSERVATION LIST

Name NGC *IC	Type	Note	Name NGC *IC	Type	Note	Name NGC *IC	Type	Note
7814	Sa		2768	S0		4631	Sc	+*
45	Sc	+*	2841	Sb	*	4725	Sb	
147	E		2903	Sc	*	4736	Sb	+*
*10	Irr	+*	3034	Irr	b*	4826	Sb	
185	Ep		Sex A	Irr	+*	5005	Sb	*
404	E		*2574	Irr	+*	5033	Sc	
628	Sc	+*	3359	SBc	+	5055	Sb	+*
672	SBc	a*	3368	Sa		5194/5	Sc/E	+*
*1727	Sc	a*	3521	Sb	*	5248	Sc	*
891	Sb	*	3556	Sc	+*	5363	Irr	
925	Sc	+*	3953	SBb		5364	Sc	
1023	S0		3992	SBb	*	5457	Sc	+*
1068	Sb	*	4192	Sb		5866	S0	*
1097	SBb	*	4216	Sb		5907	Sb	*
1156	Irr	*	4220	Sa		6015	Sc	*
1300	SBb		4236	Sc	+*	6217	Sc	*
1332	S0		4244	Sc	+*	6643	Sc	
1365	SBb	*	4258	Sb	+*	6822	Irr	+*
1569	Irr	+*	4438	Sa	*	6946	Sc	+*
1637	Sc		4449	Irr	+*	7331	Sb	*
2146	Sa	*	4490	Sc	+*	7457	E	
2336	Sb		4517	Sc		7640	Sb	+*
2537	S0	*	4565	Sb	*	7741	SBc	
Ho II	Irr	+*	4569	Sb		WLM	Irr	+c*
2683	Sb		4594	Sa	*			

* = Continuum emission detected.
+ = HI detected.
a = confusion between NGC672 & IC1727.
b = confusion with continuum
c = WLM is a Wolf-Lundmark-Melotte galaxy.

TABLE 2 CALIBRATOR FLUXES AND POSITIONS

Name	Flux	h m s	o ′ ″
0043-42	7.55	00 43 54.7	-42 24 18
3C 48	15.00	01 34 49.8	+32 54 22
3C 78	7.20	03 05 49.1	+03 55 13
3C 84	11.90	03 16 29.4	+41 19 52
3C 119	8.35	04 29 07.9	+41 32 09
0442-28	6.70	04 42 37.6	-28 15 23
0521-36	15.90	05 21 13.2	-36 30 00
3C 147	22.00	05 38 43.6	+49 49 43
3C 161	19.30	06 24 43.1	-05 51 21
3C 196	14.00	08 09 59.4	+48 22 08
3C 231	7.85	09 51 43.8	+69 54 56
3C 237	6.60	10 05 22.1	+07 44 54
3C 273	44.30	12 26 32.9	+02 19 42
3C 286	15.50	13 28 49.7	+30 45 59
3C 295	22.40	14 09 33.8	+52 26 14
3C 345	7.40	16 41 17.7	+39 54 11
3C 380	14.20	18 28 13.4	+48 42 39
3C 390.3	10.80	18 45 37.8	+79 43 03
2104-25	10.60	21 04 26.0	-25 39 30
3C 430	7.60	21 17 02.4	+60 35 27
CTA 102	6.55	22 30 07.7	+11 28 22

Note: Epoch is 1950.0 Errors in fluxes are less than 3 %. Errors in positions are less than 5" of arc. Fluxes are in units of 10^{-26} W m^{-2} Hz^{-1}.

C. Observational Techniques

1. Interferometer

A description and the predicted response of the Owens Valley twin-element interferometer are found in papers by Read (1961) and Moffet (1962). Basically the instrument consists of two elements, each a 90-foot equatorially mounted paraboloid moving on wide-gauge tracks, that can be placed at several discrete spacings (multiples of 100 feet) along an east-west or north-south baseline. The typical receiver described and analyzed by Read must be modified slightly for line studies. This involves placing a filter before the double side-band receiver to reject any signal entering at the image frequency . The basic receiver and data-recording setup used for the present observations are shown as a block diagram in Figure 1.

Tunnel diode amplifiers were used at the front end, followed by tuned cavity image rejection filters. The signal then entered the standard crystal mixers and I.F. amplifiers for conversion to an intermediate frequency of 10 MHz and further amplification. The signal from each antenna was split 13 ways, one part for a broadband channel of bandwidth about 4 MHz and the remaining parts for 12 equally spaced I.F. filters of bandwidth 100 kHz and spacing 200 kHz, where the

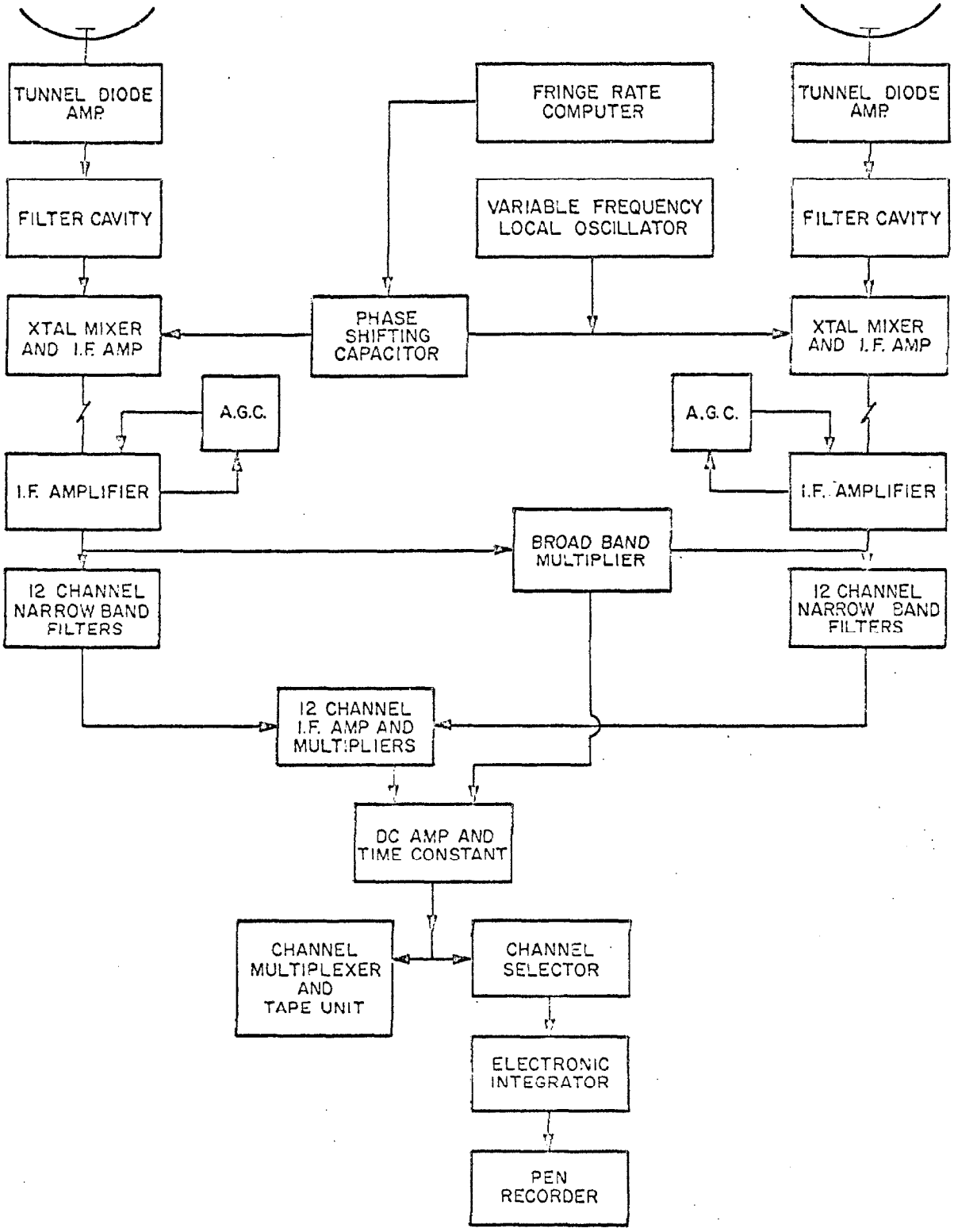

Figure 1 Block diagram of the receiver.

filters were capacity-coupled, double-tuned circuits, and their bandpass shapes were very close to a Gaussian. This means that one observation covered a frequency range of 2.3 MHz. The outputs of the filter pairs corresponding to the two antennas were then multiplied, fed through a low pass filter, and recorded on magnetic tape by sampling the signal at a certain specified time interval. The tape was reduced at a later time by computer.

A direct monitor of any given channel was provided by an electronic integrator which could sample the output signal from that channel, integrate it over the length of the observation, and continuously record the result on a pen recorder.

The response of the interferometer to a point source for the above receiver configuration is:

$$R(t) = A \cos(2\pi S \sin\theta + \psi) \tag{1}$$

where A is related to the source flux density, S is the baseline length in units of the observed wavelength, ψ is an instrumental phase error, and

$$\sin\theta = \sin d \sin\delta + \cos d \cos\delta \cos(H-h) \tag{2}$$

where d and h are the declination and hour angle of the interferometer baseline, and δ and H are the assumed declination and hour angle of the source. Any

phase ϕ remaining after Ψ has been calibrated is attributed to a difference in the actual centroid of radio emission and its assumed position in the sky. This phase is related to the differences in position by

$$\phi \simeq -2\pi S \left\{ \Delta\delta \left[\sin d \cos\delta - \cos d \sin\delta \cos(\bar{H}-h) \right] + \Delta\alpha \cos d \cos\delta \sin(\bar{H}-h) \right\} \qquad (3)$$

obtained by expanding sin θ in first order terms where $\Delta\delta$ and $\Delta\alpha$ are the declination and right ascension differences, and $\bar{H}$ is the average hour angle of the observations, all expressed in radians. This expression can also be written as:

$$\phi(r,s) \simeq 2\pi S \, r \sin\theta \qquad (4)$$

where sin θ comes from Equation (2), and r is the small distance between the radio centroid and its assumed position along this projected baseline. Since the interferometer fringes are perpendicular to the projected baseline, no information is gained about the relative positions of assumed and actual radio centroid normal to the projected baseline.

To obtain the response of the interferometer to an extended source, it is necessary to integrate the above equations over the extent of the source. Equation (1) clearly becomes:

$$R(t) = \iint_{\text{SOURCE}} T(r,q) \cos\{2\pi S \sin\Theta + \phi(r,s) + \psi'\} \, dr \, dq \qquad (5)$$

where $T(r,q)\,drdq$ is the flux density coming from a small element of the source at a distance r along the projected baseline, and q normal to the projected baseline relative to the assumed position of the source, but weighted by the antenna response pattern. As in the above equations, all distances are given in radians.

The position angle of the projected baseline measured from north to east changes with time at the rate of about $15^\circ \cos\delta$ per hour, where δ is the source declination. This implies that, for the sources at high northern declination, care must be taken to limit the time of observation to prevent smoothing out the changes of the amplitude and/or phase that occur for the corresponding changes of the projected baseline position angle.

It can be shown that Equation (5) may be written in the form:

$$R(t) = V(s) \cos\{\Phi(s) + 2\pi S \sin\Theta + \psi'\} \qquad (6)$$

where V and Φ are defined as:

$$V(s)\, e^{j\Phi} = \iint_{\text{SOURCE}} T(r,q)\, e^{j\phi(r,s)}\, dr\, dq \qquad (7)$$

which is just the one-dimensional Fourier transform of $T(r,q)$ along the projected baseline of the interferometer. The identity of Equations (5) and (6) is seen if Equation (6) is expressed in exponential form. Determination of V and Φ for several values of s allows one to invert this transform and recover the original brightness distribution $T(r,q)$ of the source, along the r direction. The complete distribution can be recovered if observations are taken for several position angles of the projected baseline.

If the dimensions of the source are not too large compared with S^{-1}, so that $\phi(r,s)$ changes only slightly with r over the source, then Equation (7) gives V and Φ which are just an average flux and phase analogous to the point-source case. It is this property of the interferometer that was used for the present observations. This result will be discussed in more detail in Section D5.

Whether Equation (1) or (6) is used to describe the interferometer response, the final result for a given antenna spacing is a quasi-sinusoid having a period varying from about 90 sec. for a 100-foot baseline down to a few seconds for the longer baselines for a source on

the equator at transit. The period of the fringes also varies with the declination and hour angle of the source. Such variation makes the choice of low-pass filter time constant, and its corresponding correction to the phase difficult, since its optimum value depends on the fringe period. The use of an analogue computer eliminated this problem. By inserting into the computer the hour angle and declination of the source being observed, it calculated the expected fringe pattern response and rotated a phase shifting capacitor at the corresponding rate. The capacitor was inserted into the local oscillator line going to one of the antennas. The effect of this phase rotation can be seen by an expansion of Ψ' in Equation (6):

$$\Psi' = -\Delta\phi_c(t) + \Psi'' \qquad (8)$$

where $\Delta\phi_c(t)$ is the fraction of a radian through which the capacitor has been turned, and Ψ'' is the remaining instrumental phase error. Plainly the capacitor can be turned just at the precise rate so as to completely cancel the natural fringe rate given by the $2\pi S \sin\theta$ term in Equation (6). An additional rotation of 2 revolutions per minute was added on top of the computed turning rate of the capacitor to give a constant 30 second fringe independent of the source being observed. To recover the natural fringe period and phase, the position of the

phase shifting capacitor was binary encoded and recorded on the magnetic tape along with the time of the sample and the actual data.

The remaining phase ψ'' is a systematic phase error due to the equipment. It varies slowly over a period of a few hours so that if calibrator sources are observed about once every hour, this error can be removed.

2. The Observations

Between the dates of May 22 and June 15, 1965, observations were carried out on the galaxies listed in Part IIB using the twin-element interferometer with a spacing of 100 feet east-west.

Before the actual observation of a galaxy could take place, it was necessary to determine two parameters. First, the observing frequency had to be calculated on the basis of the known recession velocity of the galaxy. Second, the hour angle had to be chosen to give the desired angle between the major axis of the galaxy and the projected baseline of the interferometer. It was considered desirable for interpretation to have observations with the baseline both along the major and the minor axes of the galaxy. Clearly this is only possible for the most northern galaxies, using an east-west baseline. The criterion was approached as closely as possible. The irregular galaxies, of course, could not be judged on this basis and therefore were put

into the schedule wherever convenient.

A single observation consisted of four parts. First, a calibrator was picked as close to the galaxy as possible and observed at the proper frequency for about 10 minutes. This was followed by a 20-30 minute observation of the galaxy at the same frequency. The frequency was then shifted by 100 kHz so that the frequencies between the filters were covered, and the galaxy was again observed for 20-30 minutes. Finally the same calibrator or another close by was observed for 10 minutes at this second frequency. This means that, in a one-hour observation set, a total of 24 different frequencies were observed, covering a 2.3 MHz range in 100 kHz steps. Usually channel 6, the center of the 12 channel band, was directly monitored with the electronic integrator and pen recorder. This provided a continuous check for possible noise interference, and also revealed whether or not hydrogen was being detected. If a galaxy showed signs of having a detectable signal, more observations were performed, including frequencies at 50 kHz intervals.

For all of the observations, each element of the interferometer was made to track the center of the galaxy. The effects of beam weighting and the corresponding corrections will be discussed in the next section (C3).

All 13 channels of information were recorded on magnetic tape. A multiplexer scanned through the channels serially at a sample rate of 0.2 seconds. This means that each channel was sampled once every 2.6 seconds. The tape record was broken up into 256-word blocks by the recorder. The first word, or header word, contained the record number (one for each observation to serve as an identification tag), the gain and filter constants being used, and the Pacific Standard hours and minutes of the sample. This was followed by 255 data words containing the channel number sampled, the value of the binary encoded phase-shifting capacitor, the Pacific Standard seconds of the sample, and a 10-bit binary number giving the data sample. An observation may have had as many as 40 of these blocks recorded on the tape. All other information relevant to the individual observations, such as the source corresponding to each record number and the frequency used, was recorded in a running log, so that this log together with the tape provided the observational record.

During the course of the observations, two special calibration runs were also taken. One was for the purpose of determining the interferometer baseline parameters. The other was for the purpose of obtaining an accurate and consistent set of fluxes for the

calibrators. Both of these runs are described and discussed in the next section.

3. Reduction of the Observations

The reduction technique will now be discussed. The steps in the procedure were: (a) reduction of baseline calibration run, (b) reduction of flux calibration run, (c) initial reduction of observations, (d) calibration of observations, and (e) averaging of observations. Outlines of the computer programs used in these steps are included at the end of the section. The main reduction program, called Analyz, predicted the interferometer response for a given observation and performed a least-squares fit to the data sequence using this function. The output was the amplitude, phase, and bias or d.c. level of this sequence, together with their estimated r.m.s. errors.

(a) Baseline calibration. Some of the input parameters to the main program for predicting the interferometer response are the baseline length, hour angle, and declination: s, h, and d respectively. If these are in error by the small quantities Δs, Δh, and Δd, then the first-order expansion of the interferometer response (Equation (1) and (2) in Section C1) gives a phase change for a calibrator observation of

$$\Delta\phi \simeq -2\pi\{\Delta s[\sin\delta\sin d + \cos\delta\cos d\cos(H-h)]$$

$$+ s\,\Delta d[\sin\delta\cos d - \cos\delta\sin d\cos(H-h)] \qquad (1)$$

$$+ s\,\Delta h[\cos d\cos\delta\sin(H-h)]\}$$

Therefore unknown errors in the baseline parameters will add the systematic error given in Equation (1) to the phases computed by the main program. A calibration run was performed to minimize this error. A series of calibrators from the list given in Section B were observed during the evening when the instrumental phase, ψ', was relatively constant. Any changes in phase between observations could then be attributed to the effects of Δs, Δh, and Δd. By least-squares fitting Equation (1) to the observed changes, corrections to the assumed baseline parameters were obtained. These corrected parameters were used for all subsequent reduction.

(b) Flux calibration. In order to minimize errors in calibration due to inaccuracies in the assumed flux densities of the calibrator sources, a calibrator flux density run was performed to obtain an accurate and

consistent set of fluxes. The run involved numerous short observations of only the calibrators, over the period of a day, with as much intermixing of the observations of different calibrators as possible. After initial reduction the gains (i.e. the ratio of amplitude to flux) were plotted as a function of time, and the fluxes were adjusted, assuming a fixed value for 3C295, to obtain the smoothest gain-time curve. Possible gain correlations with observation hour-angle or declination were also checked and found negative. The flux densities that were determined are those quoted in Table 2 of Section B. The value for 3C295 is from Kellermann (1964).

(c) Initial Observation Reduction. All galaxy observations were then reduced, again using the main program. At this time problems of noise interference were cleared up by either rejecting an observation or cutting out the bad sections of the record. The output consisted of a punched card containing the results of each channel for each observation.

(d) Calibration of Observations. Two possible methods of calibration were considered. First, the phase and gain time-smoothed curves from the main program could be used to correct the source phases and fluxes. Because of some phase and gain variations with frequency due to the front-end filter cavities, this method was dropped in

favor of the second. This method used a weighted linear time interpolation between the phases and gains of the calibrators before and after each source observation. While the first method would involve smoothing the phase and gain determined at perhaps widely varying frequencies, the second involved calibrators observed at the same frequency as the galaxy with no more than a 100 kHz frequency change. This small variation was neglected. Using this method, the observations were calibrated with the final results appearing in the form of flux and phase at each frequency together with their estimated errors.

(e) Averaging procedure. Since several observations were taken of many of the galaxies, it was necessary to average them to obtain a final line and position profile. At the time of observation, the changes of recessional velocity due to the earth's motion around the sun was not considered, so that observations taken at the same frequency, but separated in time by several days, were effectively taken at different recessional velocities. Therefore, when these observations were averaged, their small spread in velocity effectively increased the bandwidth of the final average. This increase was less than 5 km/sec. When it was decided to average adjacent channels for some of the galaxies, the increase was about 12 km/sec.

After the observations were processed by the

averaging program, the results were studied carefully to decided whether or not HI had been detected. A few of the observations were rejected because of obvious noise interference that had passed previous inspection, or in cases where the antennas were mis-directed for one set and no signal was recorded. With all corrections made the whole set was processed again.

Two steps in the program should be discussed here. (1) The broadband channel gave a very accurate estimate of the continuum emission entering the antenna beam. The line was contained within this frequency band, but was sufficiently narrow in comparison to the bandwidth, or the HI region sufficiently large compared to the fringe spacing as to give a negligible contribution to the continuum flux density. Assuming no differential hydrogen absorption took place across the extent of the continuum source, this continuum emission was subtracted vectorially from the narrowband channels to leave only the hydrogen line and position profiles. Since all the observations were taken over a fairly wide frequency range, many fell outside the line profile. Subtraction of the continuum from these left essentially noise, which quite consitently represented the expected flux and phase noise errors estimated by the main program.

(2) Since the antennas were pointed only at the optical center of each galaxy during the course of an observation, the flux density from hydrogen off the galaxy's center was diminished by beam smoothing. The beam pattern was very closely approximated by a Gaussian of 16.5 of arc halfwidth. An approximate correction was made for this effect by increasing the flux in each channel by the beam pattern factor corresponding to the centroid position of the hydrogen contributing to the channel. This, of course, was applied only when hydrogen was definitely detected.

(f) Outlines of Programs. The programs used in the above reductions were coded in Fortran IV and IBMap programming languages for use on an IBM 7094 digital computer.

Analyze Program

A. Main control section - Link 0

1. Read in option control flags.
2. Read in source position and flux table.
3. Read in multichannel parameters.
4. Begin reduction by day by reading in date, Independent day numbers, and tape file number.
5. Call reduction section of program.
6. Call calibration section of program.

7. Return to statement (4) until all days are completed.

B. Reduction section - Link 1

1. Read in tape unit assignments and use file and record numbers to position tape.
2. Read source observation card containing name, observing frequency, clock errors, etc. Read time correction card for time of noise interference.
3. Search source position table for position and precess to date of observation.
4. Read tape record, rearrange data into channel blocks and write onto disc file.
5. Call data off disc file by channel and process to obtain raw amplitude and phase of observation. Tape sections containing noise interference are not processed.
6. Correct amplitude and phase for low-pass filters and gain.
7. Print out and punch on cards all results.
8. Return to statement (2) until all sources for given day are complete.
9. Return to Link 0.

C. Calibration section - Link 2

1. Obtain names and observational results of

calibrators for given day from common storage with Link 1.

2. Fill spatial plotting arrays and plot curves of calibrator phase and gain versus time of day.
3. If baseline calibration option is desired, call this section which uses least-squares fitting procedure to obtain baseline length and orientation corrections. This is done on broadband channel only.
4. Punch decks of phase-time and gain-time smoothed curves.
5. Return to Link 0.

In step B6 corrections are made to the amplitude and phase due to the effects of the low pass filter. The filter was a simple 5 sec R.C. time constant, so that the phase correction is simply:

$$P_{COR} = \tan^{-1}(2\pi\tau/PER.)$$

and the gain correction is:

$$G_{COR} = \sqrt{1 + (2\pi\tau/PER.)^2}$$

where τ is the time constant and PER is the period of the sine wave. PER is calculated in step B5.

Final Calibration Program

1. Read in calibrator flux table.
2. Read in cards from main program for one observation set (i.e. calibrator, source, source, calibrator).
3. Determine gain from amplitude and the flux of calibrator obtained from flux table.
4. Linearly interpolate between calibrator gain and phase (a time interpolation), weighting each observation by its signal to noise ratio (i.e. amplitude divided by r.m.s. noise).
5. Calibrate corresponding source observations with resulting calibration curve and re-estimate amplitude and phase errors with added calibration uncertainty.
6. Punch all results on cards.
7. Return to (2) until all sets are completed.

Averaging Program

1. Read in position table.
2. Read in all observations for one galaxy at one position angle.
3. Convert frequency to velocity and correct to Sun, using source position, hour angle, and date.

4. Do vector average (flux = r, phase = θ) of observations with radial velocities within specified interval.
5. Convert phase to position in sky along projected baseline, and correct flux for beam attenuation.
6. Subtract vectorially the broadband continuum emission.
7. Print out all observations and averages.
8. Plot line and position profiles.
9. Return to (2) until all observations are complete.

4. Results

Of the 75 galaxies searched for neutral hydrogen in the present survey, 25 were found to have a detectable signal. The results of these 25 are shown in Figure 2. While the bandwidth of the filters used was always 100 kHz or 22 km/sec., the effects of averaging increased it to about 28 km/sec. or greater. The bandwidth is best represented as 28 km/sec. or the distance between successive points in the line profile, whichever is greater.

The position profile gives the distance along the projected baseline of the interferometer with respect to the position given in the figure as a function of radial velocity. When the position angle of the major axis of the galaxy was known, and the difference between it and the position angle of the projected baseline was less

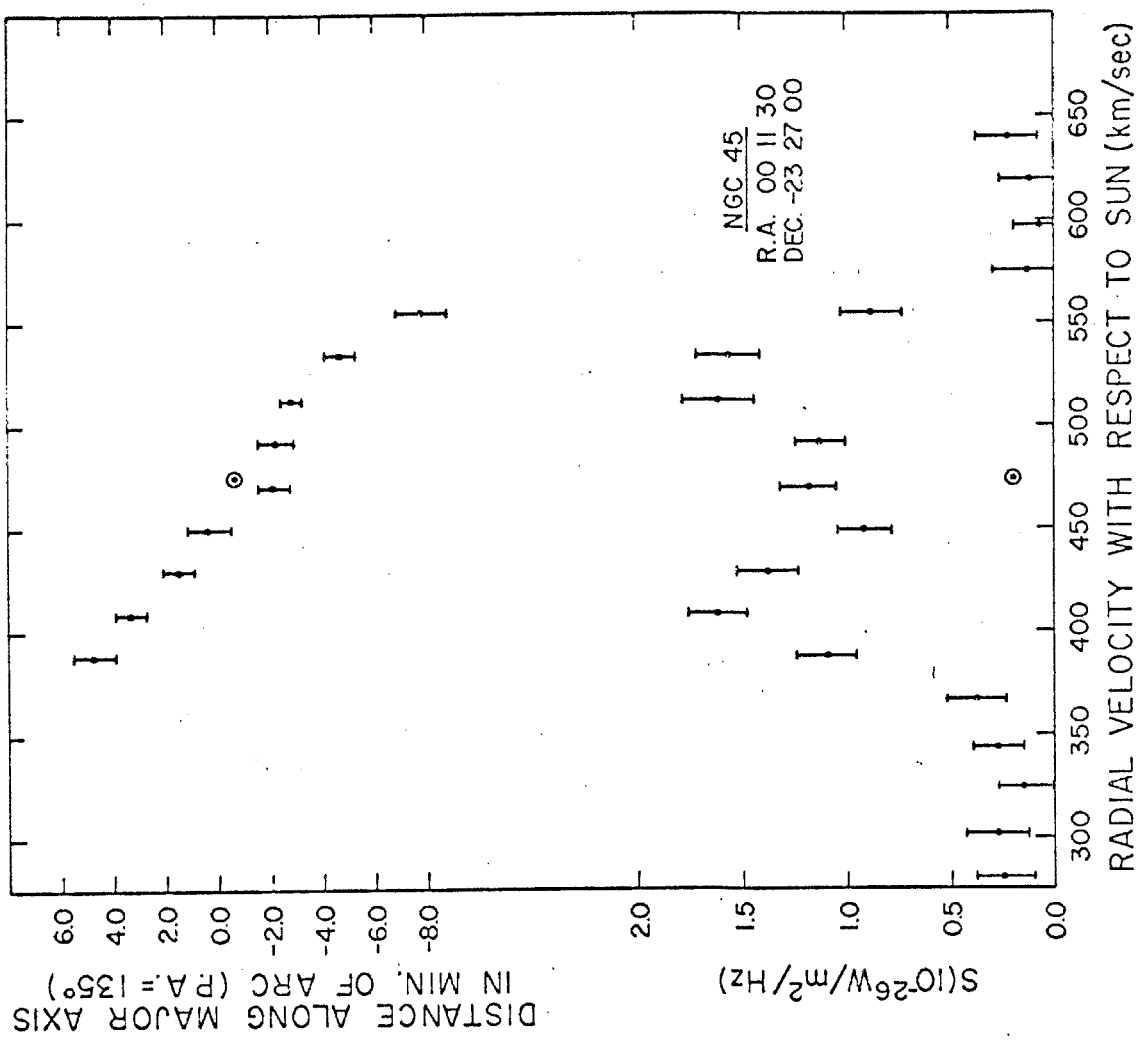

Figure 2 Line and position profiles for 25 galaxies. Circled points are continuum results. The bandwidth is 28 km/sec or the distance between successive points, whichever is greater. Positions are Epoch 1950.

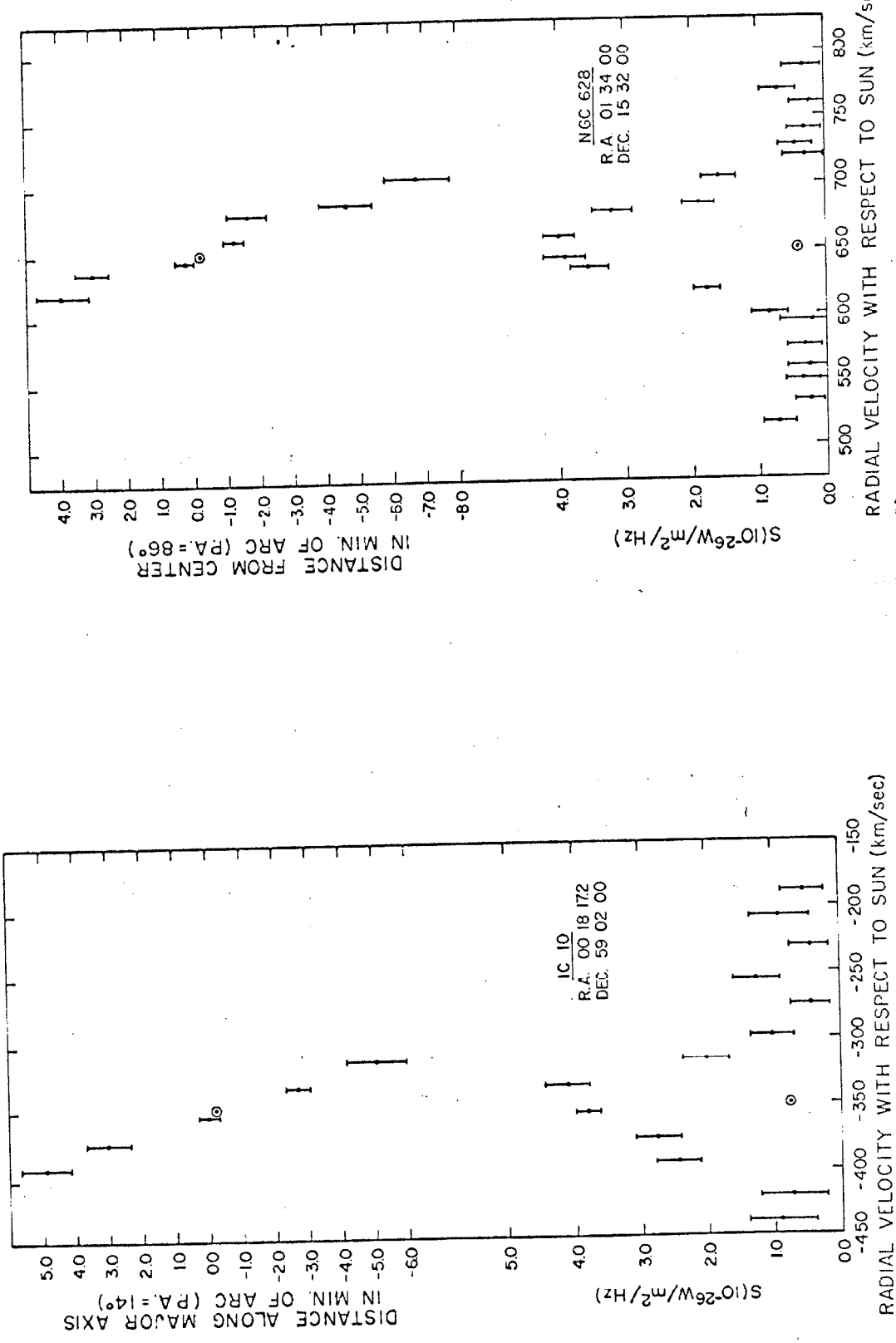

Figure 2 (continued)

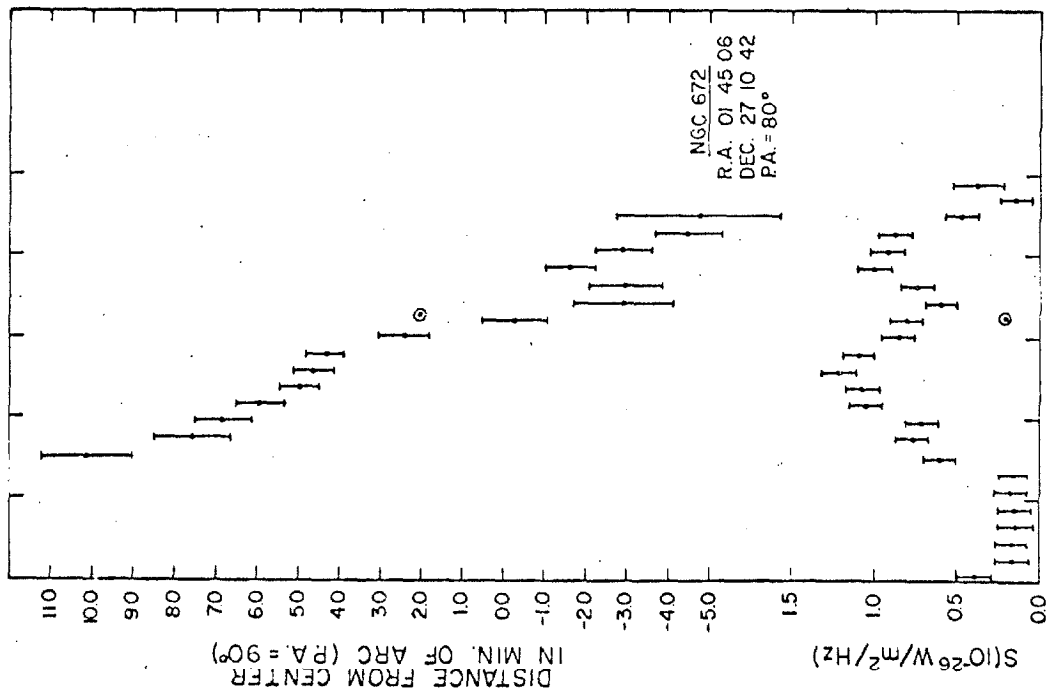

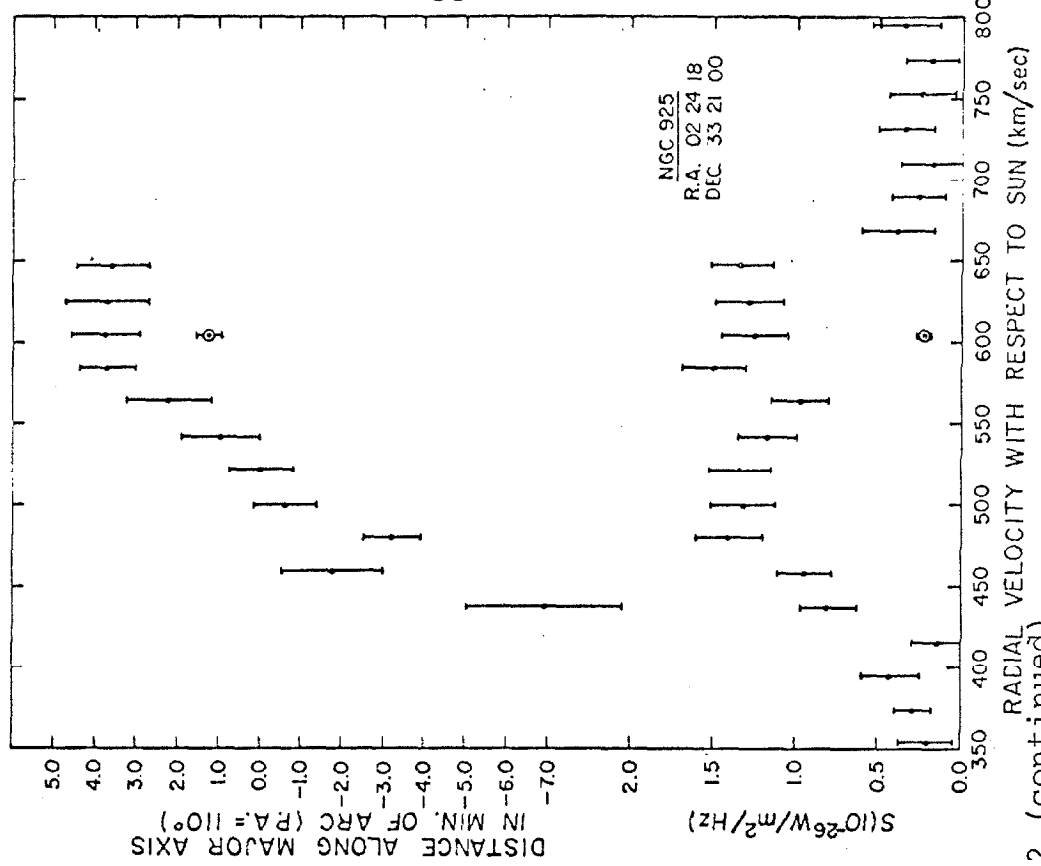

Figure 2 (continued)

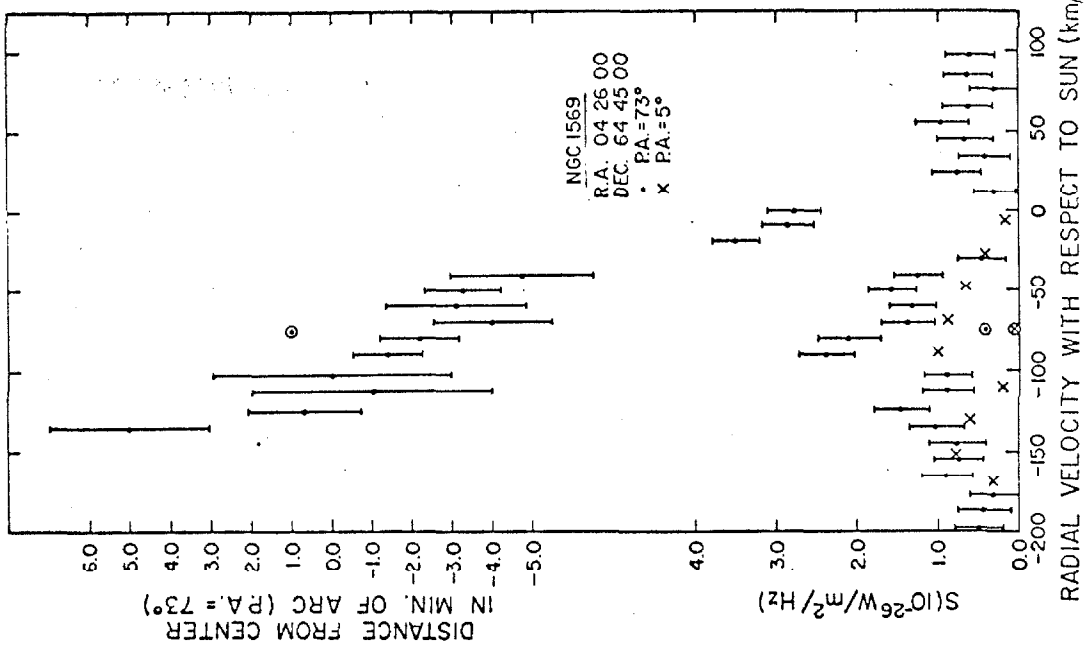

Figure 2 (continued)

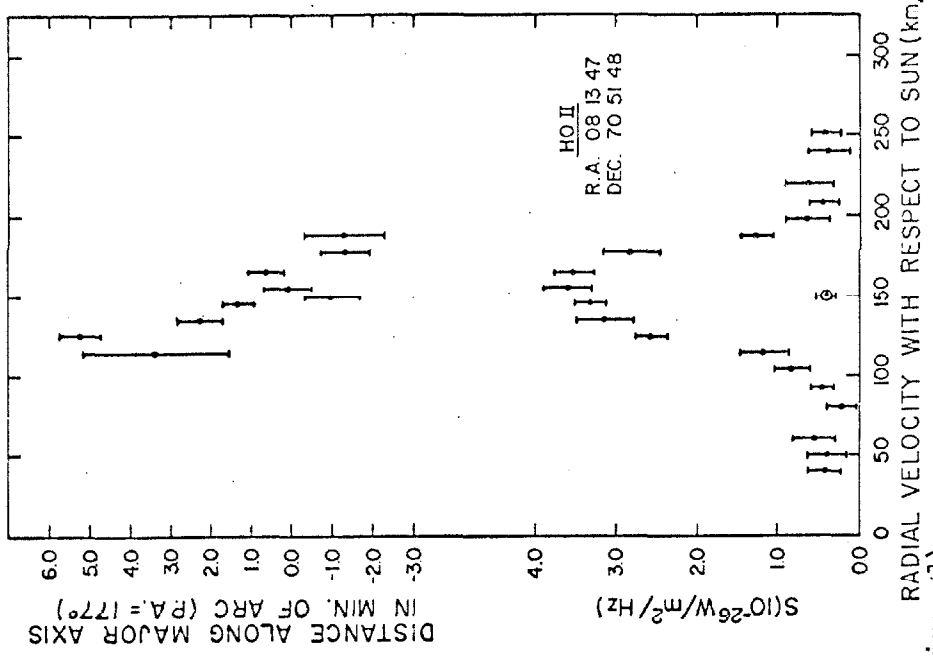

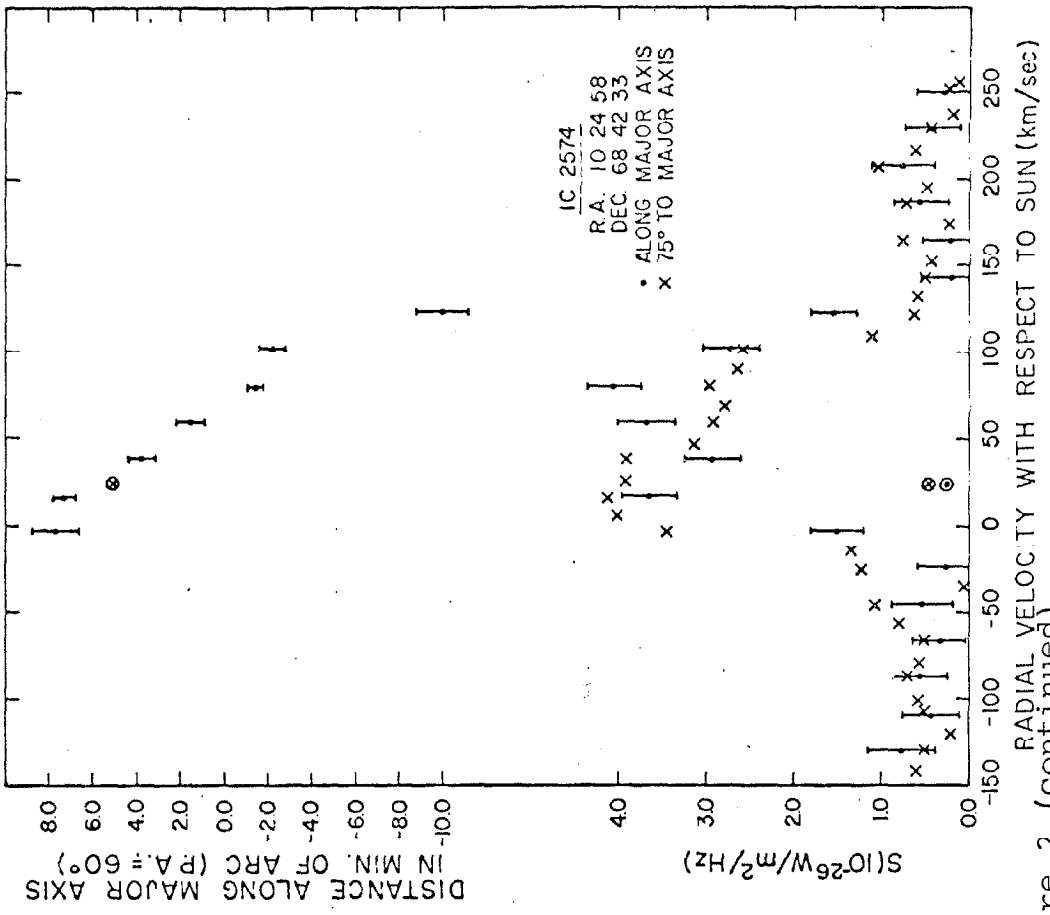

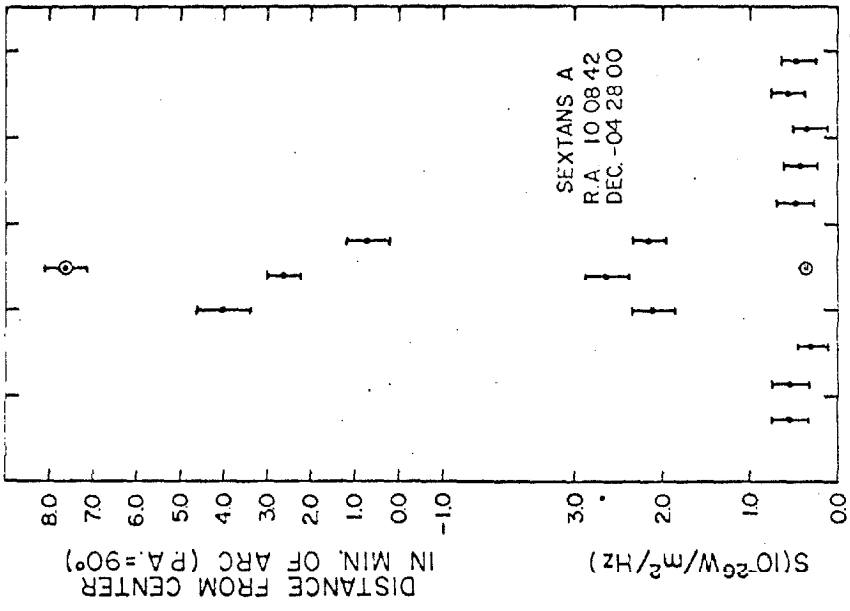

Figure 2 (continued)

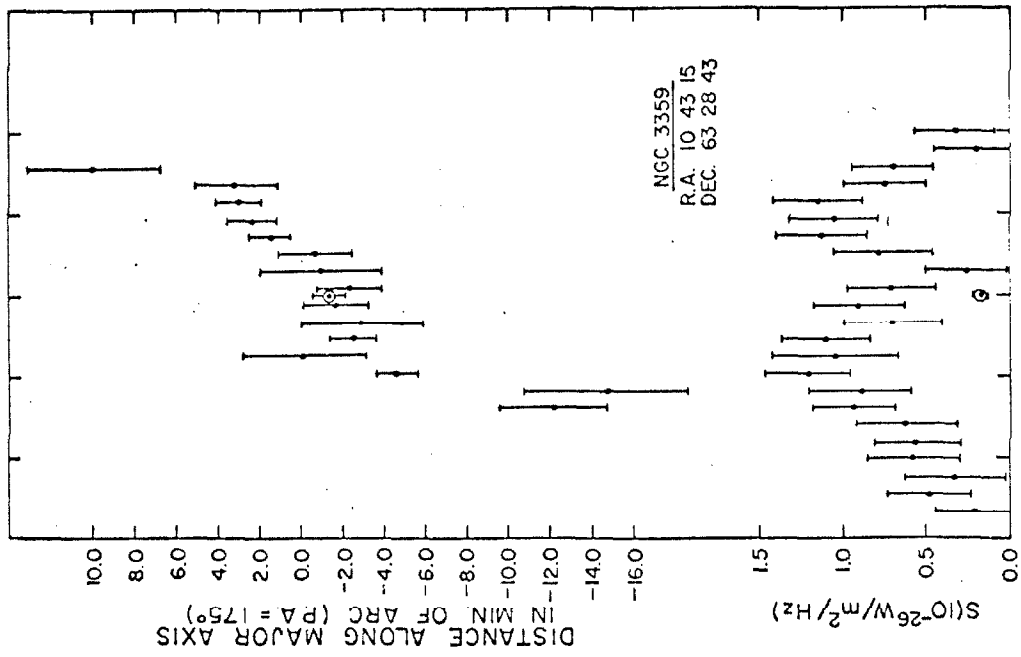

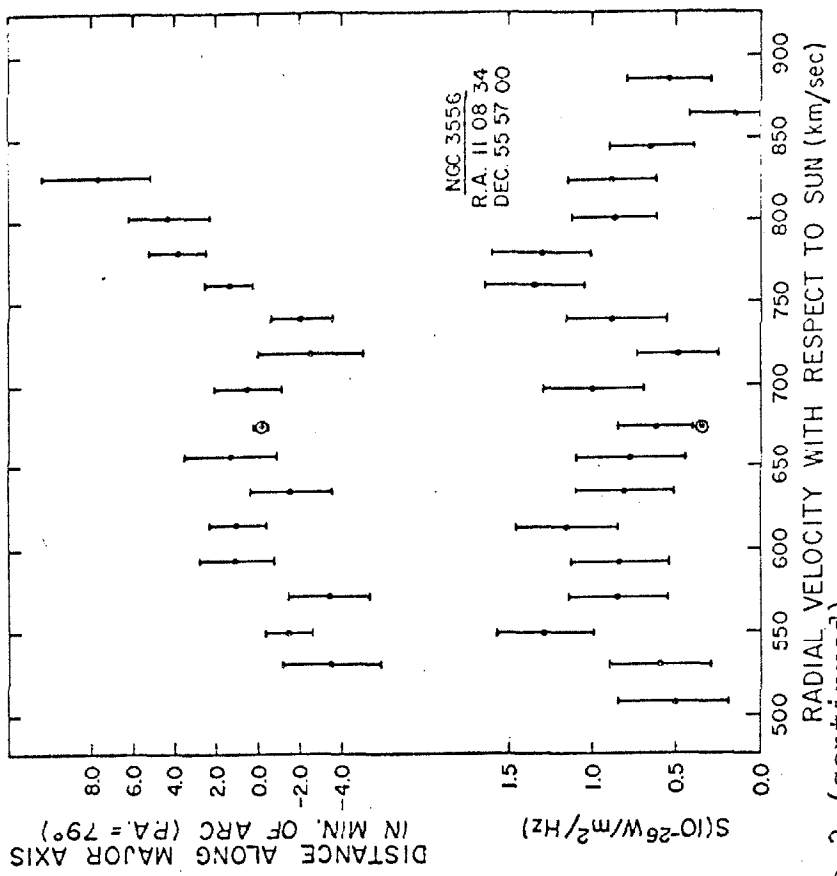

Figure 2 (continued)

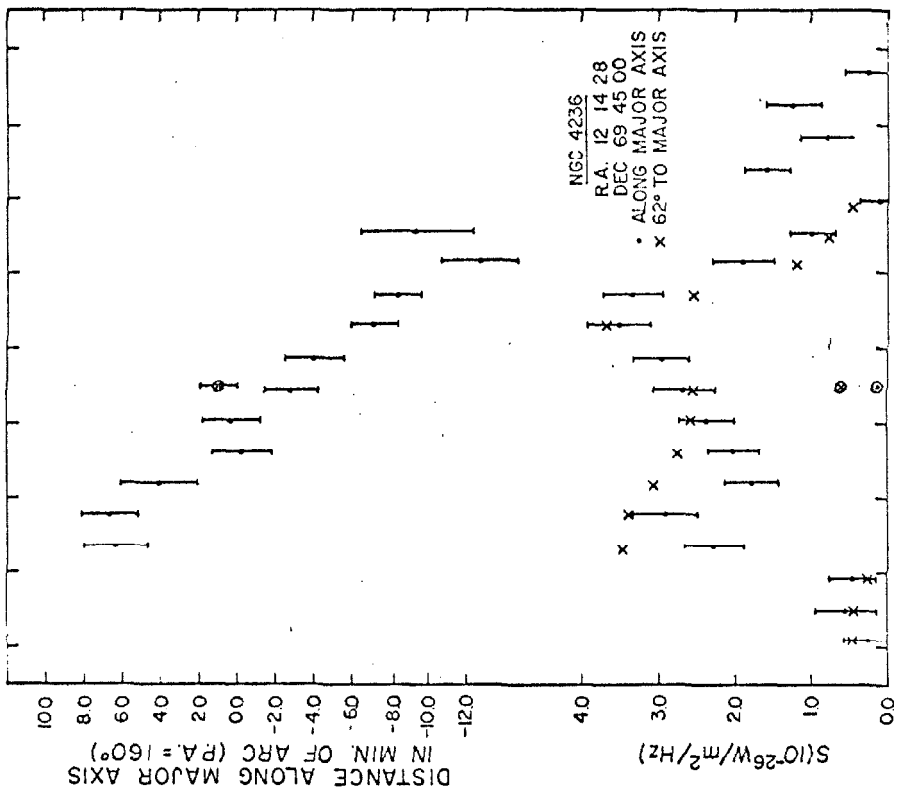

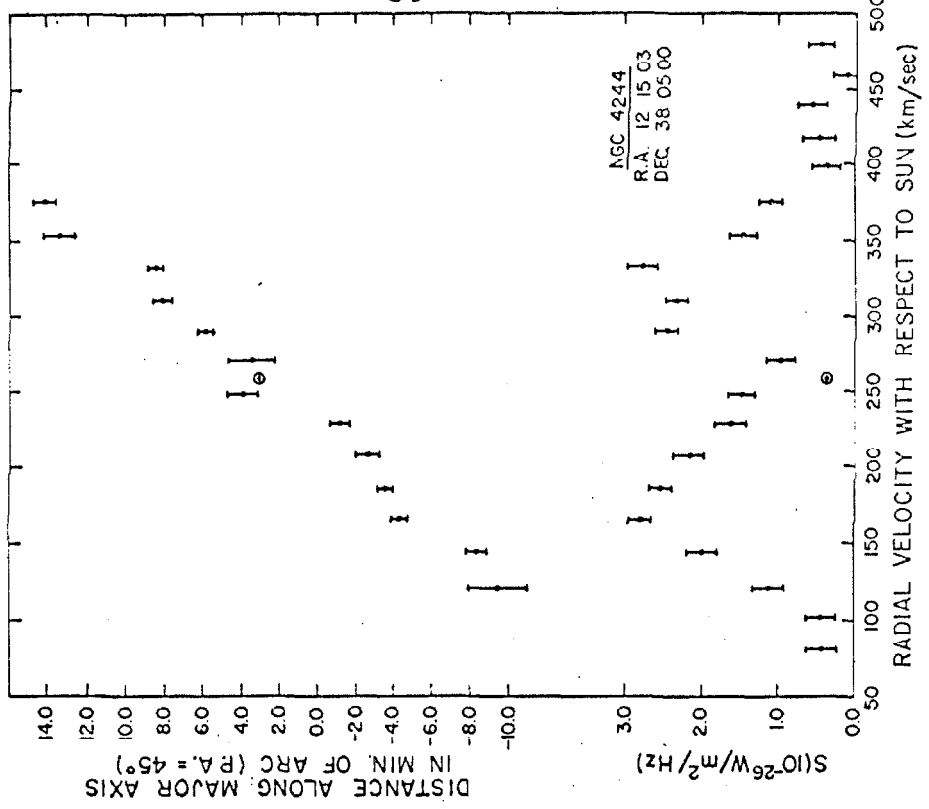

Figure 2 (continued)

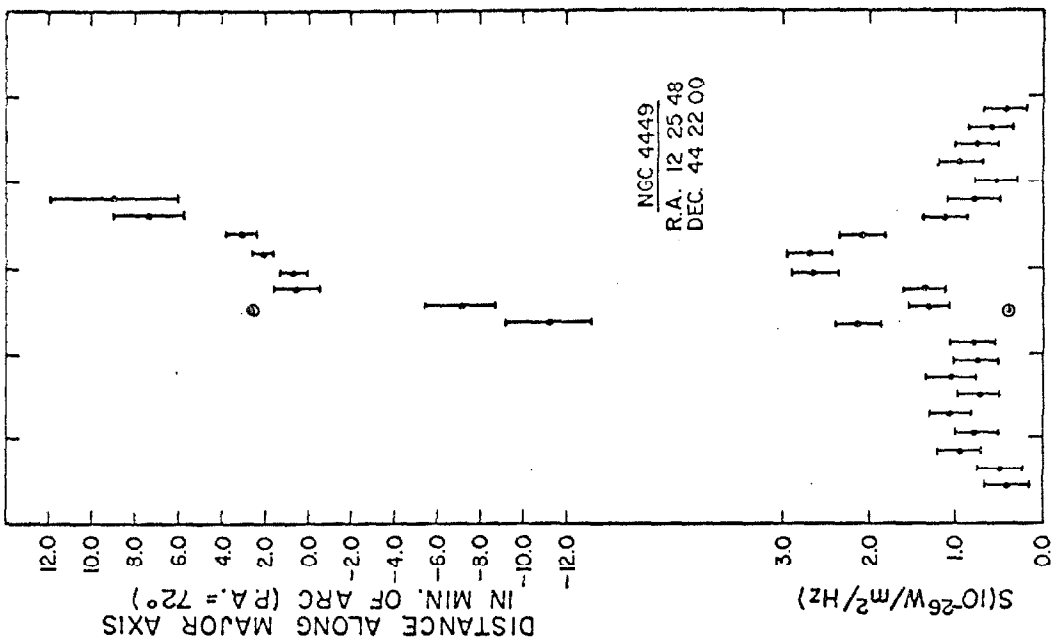

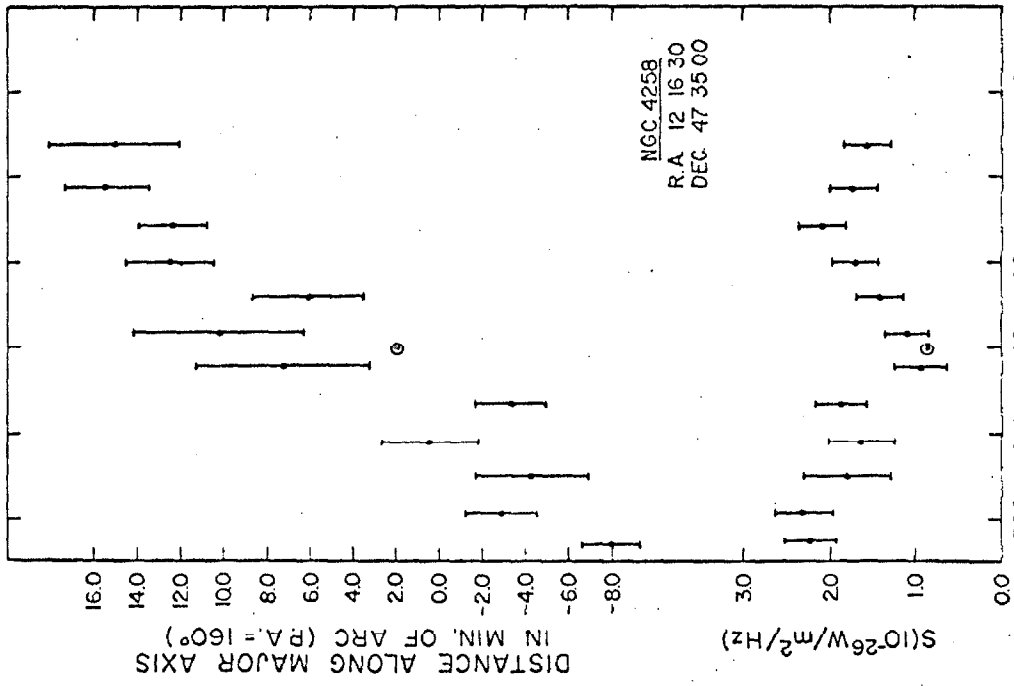

Figure 2 (continued)

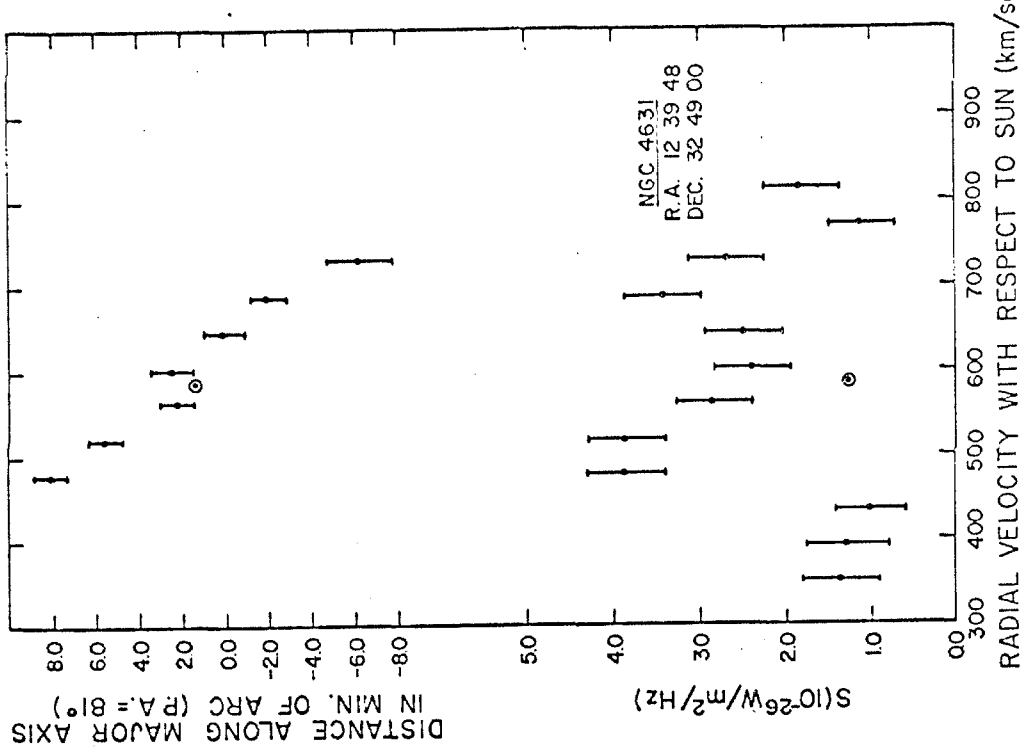

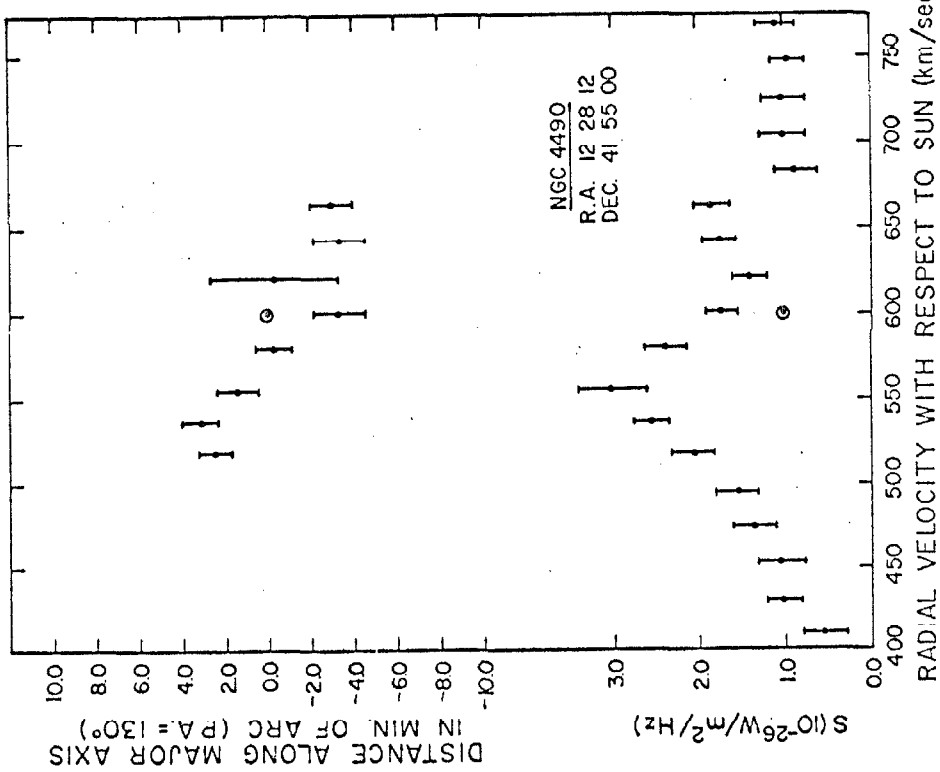

Figure 2 (continued)

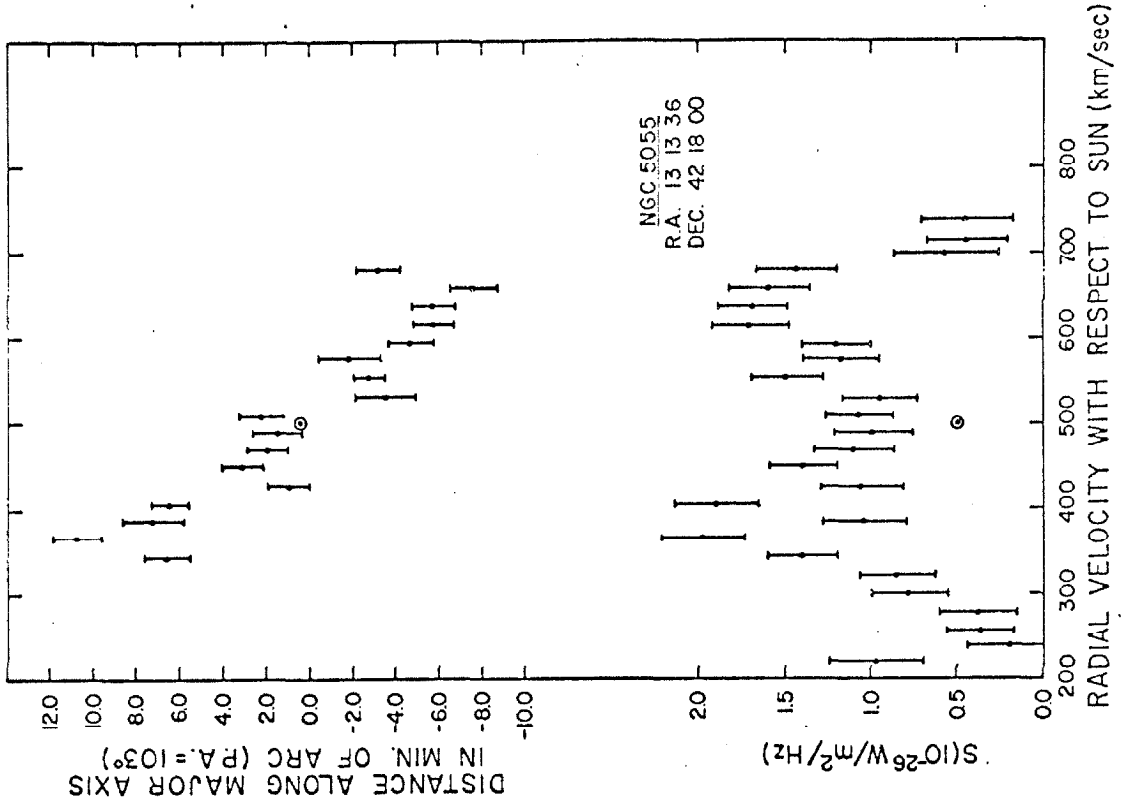

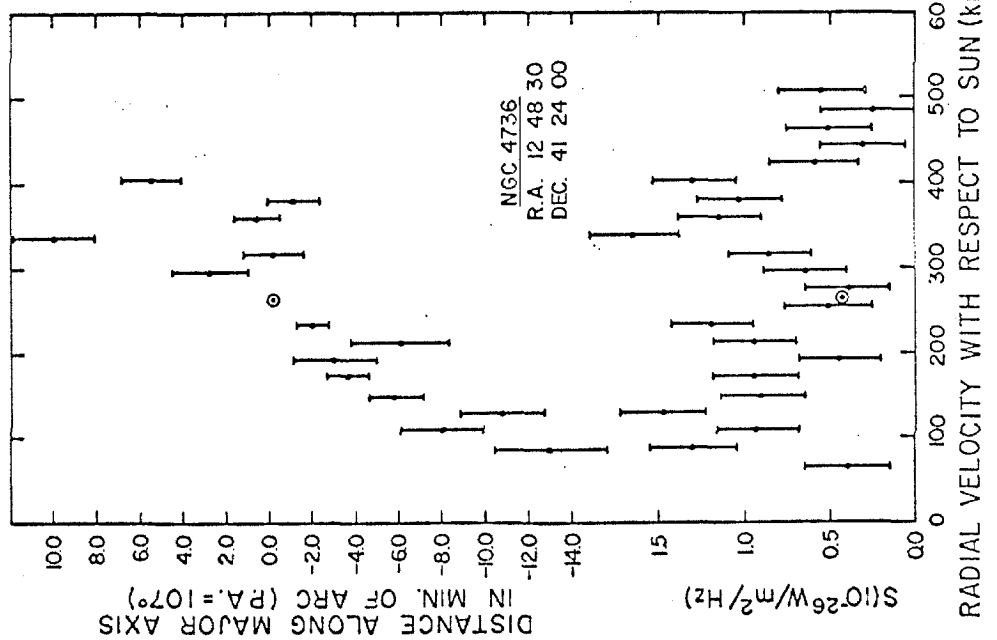

Figure 2 (continued)

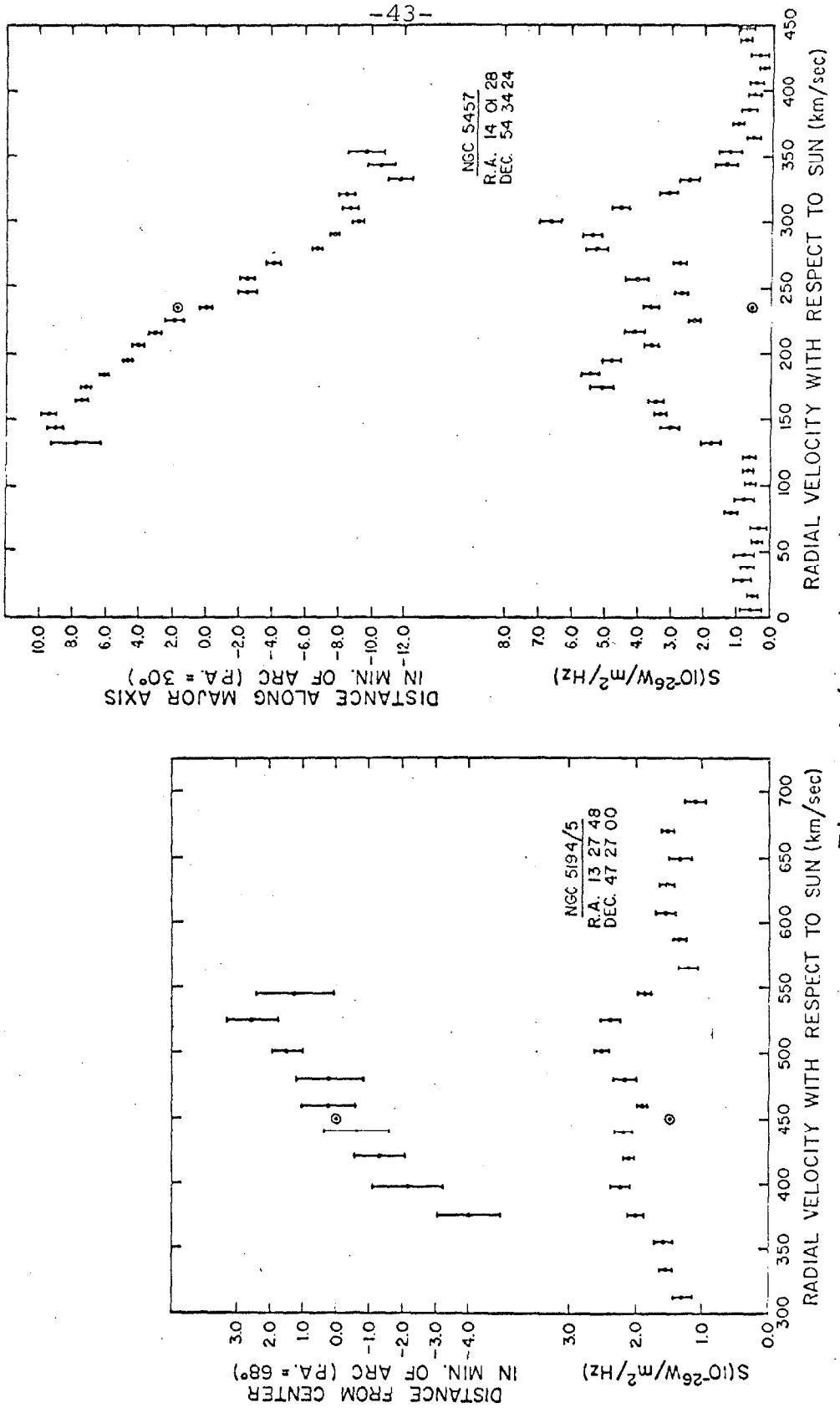

Figure 2 (continued)

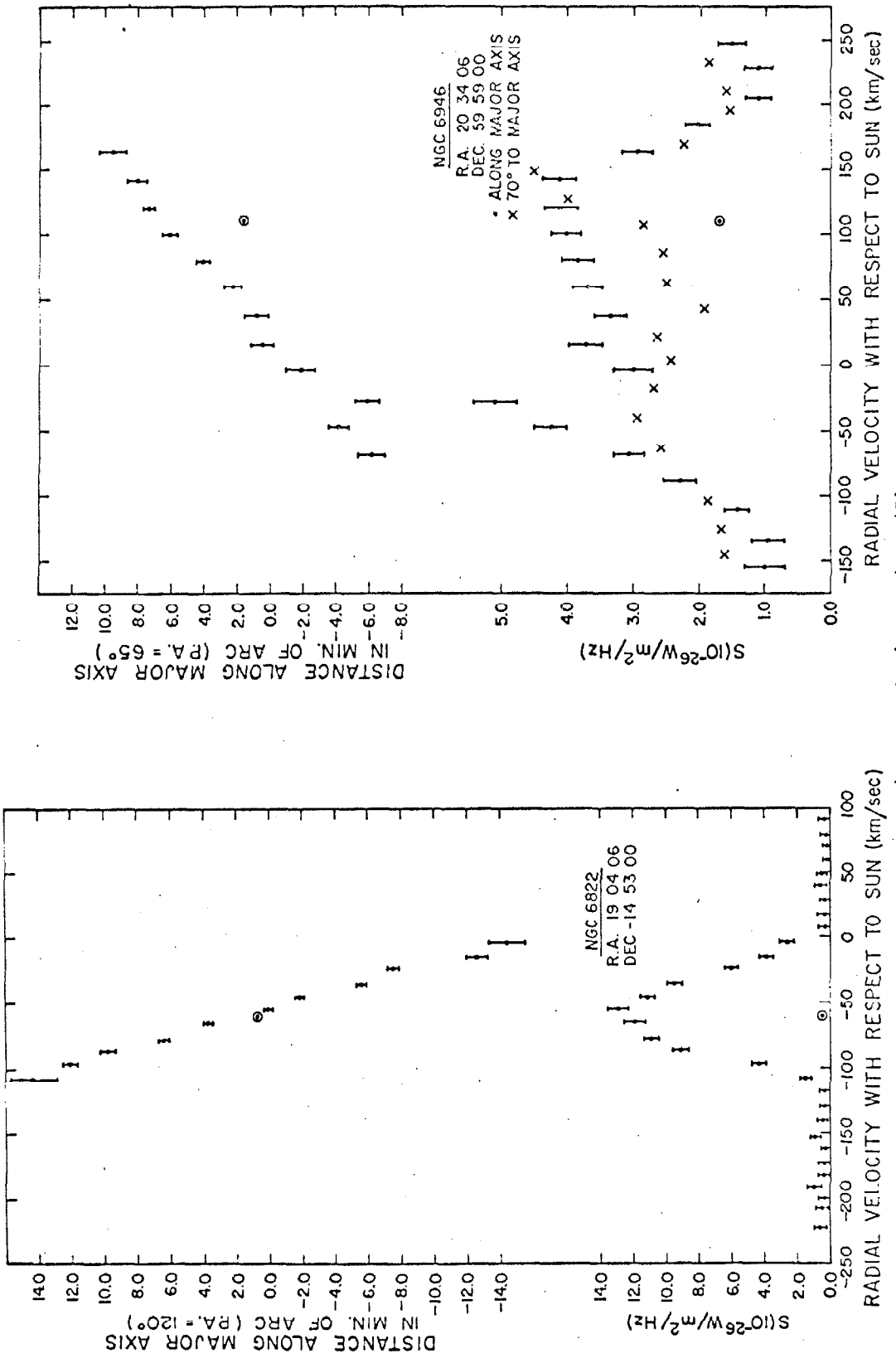

Figure 2 (continued)

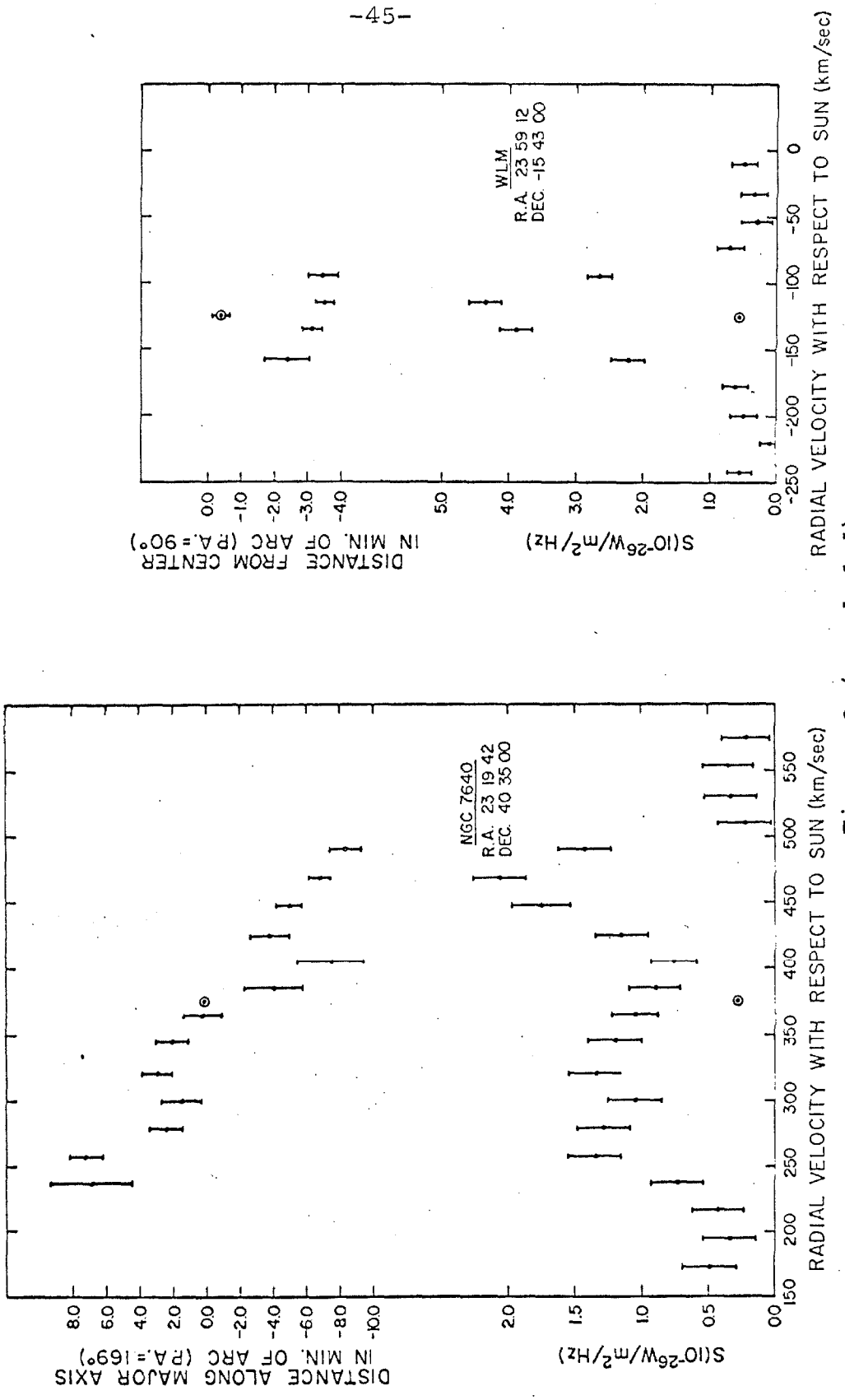

Figure 2 (concluded)

than 15°, then the positions were corrected for the cosine of this difference angle and given as along the major axis of the galaxy. For some of the galaxies, it was possible to calculate a position angle of the major axis from the observational results. The change in slope of the position profile for different projected baseline position angles was assumed to be directly proportional to the sine of angle between the major axis of the galaxy and the projected baseline, and for the galaxies having observations at several orientations of the projected baseline, rough estimates of the major axis position angles were made. This was done for IC10, Holmberg II, and IC2574. No other estimates were available for comparison.

Table 3 summarizes some of the results and parameters of the galaxies that were detected. Column 1 contains the name of the galaxy, column 2 the type, column 3 the position angle of the major axis if known or derived. The position angle for NGC6822 was taken from Volders and Högbom (1961), and the rest were taken from Danver (1942). Column 4 contains the estimated recession velocity with respect to the Sun. This velocity was determined by estimating the center of the position profile and noting its corresponding velocity. Its errors are believed to be less than ±20 km/sec.

Table 4 contains a list of the galaxies for

TABLE 3 GALAXIES CONTAINING DETECTABLE H I

Name NGC *IC	Type	P.A. of Major Axis	V_{HI} (km/s)
45	Sc	135	+470
*10	Irr	14[a]	-350
628	Sc	0[b]	+655
672	SBc	80[c]	+420
925	Sc	110	+555
1569	Irr	-	-90
Ho II	Irr	117[a]	+150
Sex A	Irr	-	+320
*2574	Irr	60[a]	+45
3359	SBc	175	+1010
3556	Sc	79	+670
4236	Sc	160	+5
4244	Sc	45	+245
4258	Sb	160	(+450)
4449	Irr	72	+190
4490	Sc	130	+590
4631	Sc	81	+600
4736	Sb	107	+240
5055	Sb	103	+510
5194/5	Sc/E	42	+455
5457	Sc	30	+235
6822	Irr	120[d]	-57
6946	Sc	65	+45
7640	Sb	169	+370
WLM	Irr	-	-130

Notes:
a = P.A. calculated from data.
b = Slope of position profile suggests P.A. is closer to 90°.
c = Position profile was not projected to this P.A. because of confusion with IC 1727.
d = P.A. from Volders and Hogbom (1961).

TABLE 4 GALAXIES NOT DETECTED
WITH UPPER LIMITS ON THE HI FLUX

Name NGC *IC	Type	HI flux limit	Search range (km/s)	Name NGC *IC	Type	HI flux limit	Search range (km/s)
7814	Sa	0.4	766,1316	3992	SBb	0.5	757,1257
147	E	0.5*	-515,35	4192	Sb	0.5	-405,95
185	E	0.5	-516,35	4216	Sb	0.5	-250,250
404	E0	0.5*	-334,166	4220	Sa	0.5	710,1210
*1727	Sc	a		4438	Sa	0.5	-308,192
891	Sb	0.3	-177,323	4517	Sc	0.5	890,1390
1023	S0	0.5	290,790	4565	Sb	0.5	925,1425
1068	Sb	0.5	770,1270	4569	Sb	0.5	660,1160
1097	SBb	0.3	1062,1562	4594	Sa	0.5	820,1320
1156	Irr	0.5*	142,642	4725	Sb	0.5	800,1300
1300	SBb	0.5	1390,1890	4826	Sb	0.5	100,600
1332	S0	0.5	1340,1840	5005	Sb	0.5	707,1207
1365	SBb	0.5	1386,1886	5033	Sc	0.5	628,1128
1637	Sc	0.5	440,940	5248	Sc	0.5	905,1405
2146	Sa	0.3	640,1140	5363	Irr	0.5	855,1355
2336	Sb	0.5	2132,2632	5364	Sc	0.5*	1104,1604
2537	S0	0.5	110,610	5866	S0	0.5	458,958
2683	Sb	0.4	35,535	5907	Sb	0.5*	295,795
2768	S0	0.5	690,1190	6015	Sc	0.5	367,867
2841	Sb	0.3	283,783	6217	Sc	0.6	1108,1608
2903	Sc	0.7*	324,824	6643	Sc	0.3	1226,1726
3034	Irr	b		7331	Sb	0.3	580,1082
3368	Sa	0.5	650,1150	7457	E	0.4	277,777
3521	Sb	0.5*	494,994	7741	SBc	0.5	500,1000
3953	SBb	0.5	678,1178				

Flux limit is in units of 10^{-26} W $m^{-2}Hz^{-1}$.
* Possible HI detection.
a Confused with NGC 672.
b Confused with large continuum.

which the detection of hydrogen was doubtful or definitely negative. Column 1 contains the name of the galaxy, column 2 its type, column 4 the range in velocity over which the search was made, and column 3 the upper limit on the hydrogen signal.

5. Errors and the Detection Limit

The errors for the present observations can be divided into two groups: (a) The uncertainties arising from errors in the observations themselves; (b) the uncertainties arising from improper or inexact interpretation of the observations. The first group will be discussed here, and the second group in Section E.

The observational errors can be further subdivided into random, accidental, and systematic errors.

(a) Random errors. The primary source of errors for the present observations was the random (i.e. different from observation to observation) uncertainty arising from the noise of the receiver. The origin of this noise was the front end of the receiver where most of the amplification took place. The overall receiver temperature was measured by observing the change in total detected power as the antennas were moved on and off of a source of known brightness temperature. The temperature measured was about 600°K. The equivalent noise flux for a half hour observation through the 100 kHz filters was about

0.4 flux units (10^{-26} w $m^{-2}Hz^{-1}$). For each observation, an estimate of this noise was made by calculating the r.m.s. deviation of each sample data point from the final calculated response curve obtained from the least-squares fit. The average of these estimates was essentially equal to the value obtained above.

The effect of this noise on the amplitude and phase of the signal will now be considered. The response of the interferometer is described quite well by the sum of a sinusoid and Gaussian noise. The diagram

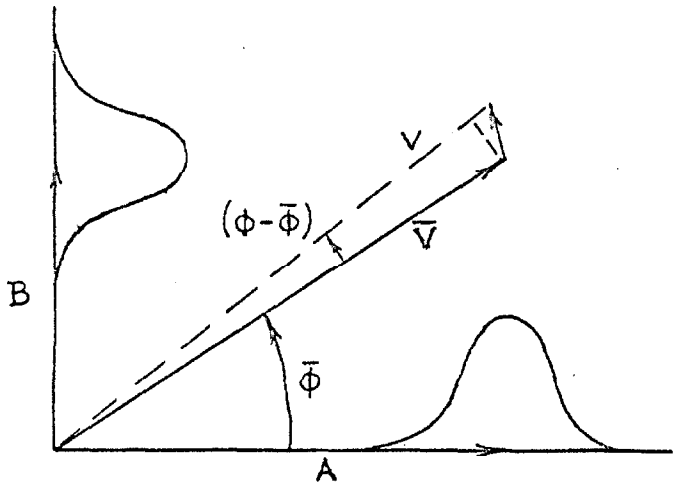

shows the two normally distributed components of the response which can be written:

$$A(t) = V(t)\cos\phi(t) \qquad (1)$$

and

$$B(t) = V(t) \sin \phi(t) \tag{2}$$

where the response is:

$$R(t) = V(t) \cos(\omega t + \phi(t)) \tag{3}$$

The noise is mixed into V and ϕ such that A and B are normally distributed. Following an analysis similar to Davenport and Root (1958), the probability density of finding any given A and B is the product of the two densities for $A(t)$ and $B(t)$:

$$P(A,B) = \frac{1}{2\pi} \frac{\exp\left[-\frac{(A-\bar{V}\cos\bar{\phi})^2}{2\sigma^2}\right]}{(2\pi\sigma^2)^{1/2}} \frac{\exp\left[-\frac{(B-\bar{V}\sin\bar{\phi})^2}{2\sigma^2}\right]}{(2\pi\sigma^2)^{1/2}} \tag{4}$$

where $\bar{V}$ and $\bar{\phi}$ are the true noiseless values of $V(t)$ and $\phi(t)$ and it is assumed that $A(t)$ and $B(t)$ have the same standard deviation σ. We are interested in the distribution of V and ϕ. Clearly we can write

$$P(V,\Phi)\, dV\, d\phi = p(A = V\cos\phi, B = V\sin\phi)\, dA\, dB \tag{5}$$

But since the area element $dA\,dB$ is:

$$dA\,dB = V\,dV\,d\phi \tag{6}$$

we get for the joint probability density of V and ϕ :

$$P(V,\phi) = \frac{V}{4\pi^2\sigma^2} \exp\left[-\frac{V^2+\bar{V}^2 - V\bar{V}\cos(\phi-\bar{\phi})}{2\sigma^2}\right] \tag{7}$$

for $V \geq 0$ and 0 for $V < 0$.

This density function can be integrated over all the angles to give the probability density for V alone:

$$p(V) = \frac{V}{\sigma^2} \exp\left[-\frac{V^2+\bar{V}^2}{2\sigma^2}\right] I_o\left(\frac{V\bar{V}}{\sigma^2}\right) \quad \text{for } V \geq 0 \tag{8}$$

where $I_o(x)$ is the zero-order Bessel function of imaginary argument. A plot of this function for several values of $\bar{V}/\sigma$ is seen in Figure 3b. A similar probability density can be obtained for ϕ alone by integrating over V:

$$P(\phi) = \frac{1}{4\pi^2} \exp\left[-\frac{V^2}{2\sigma^2}\right] + \frac{V\cos(\phi-\bar{\phi})}{4\pi^2\sigma} \exp\left[-\frac{V^2\sin^2(\phi-\bar{\phi})}{2\sigma^2}\right] K\left[\frac{\bar{V}\cos(\phi-\bar{\phi})}{\sigma}\right] \tag{9}$$

where

$$K(z) = \int_{-\infty}^{z} \exp\left(-\frac{u^2}{2}\right) du$$

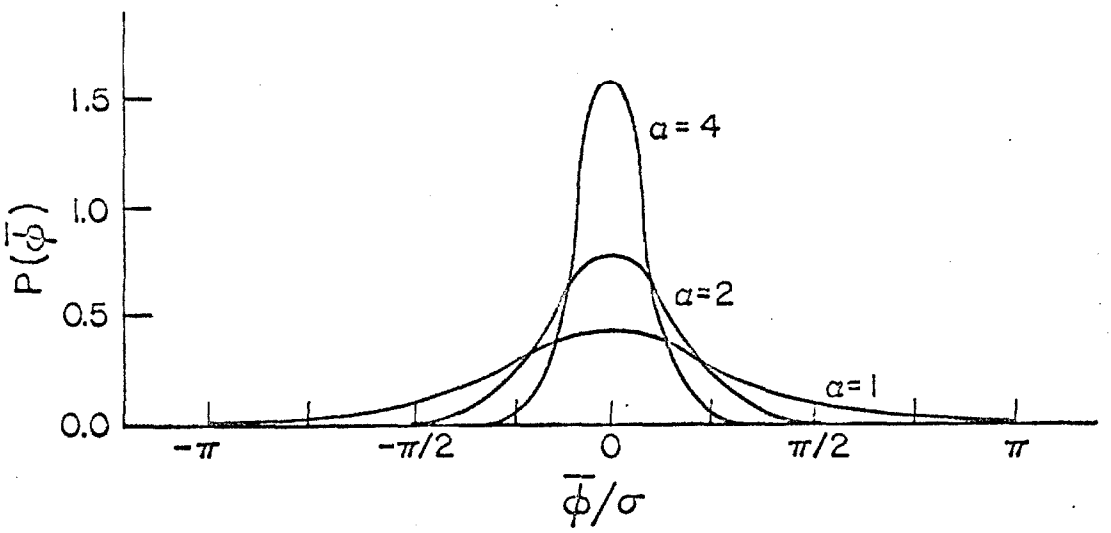

(a) PROBABILITY DENSITY FOR PHASE

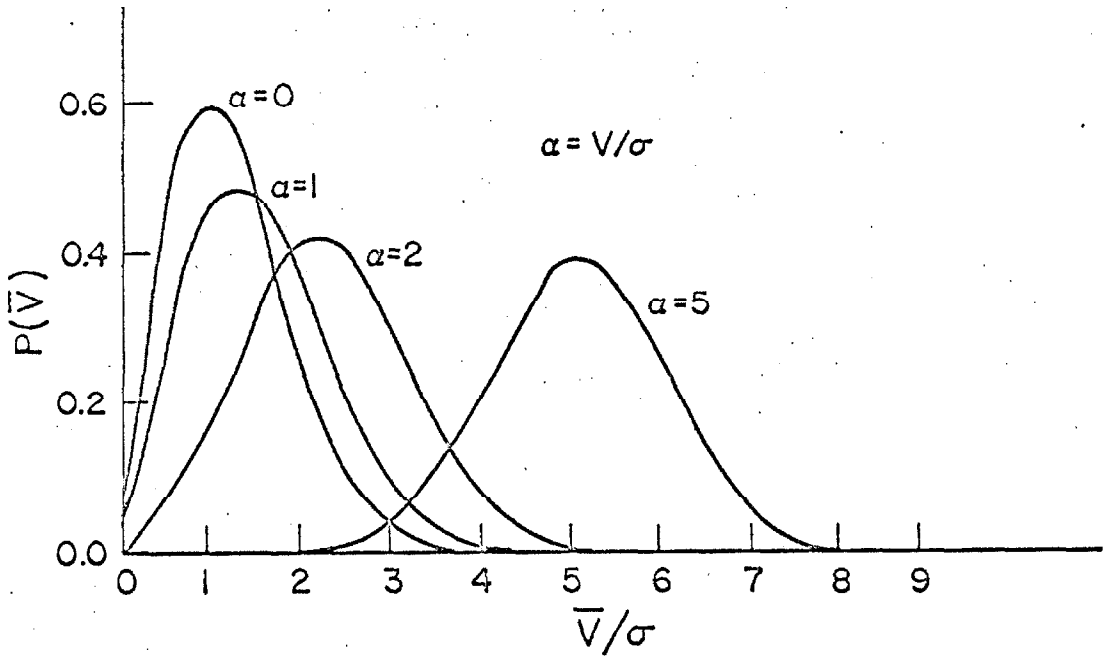

(b) PROBABILITY DENSITY FOR AMPLITUDE

Figure 3 Probability Distributions of Amplitude and Phase in the presence of noise.

A plot of this function for several values of $\bar{V}/\sigma$ is found in Figure 3a.

From the figures it is evident that for small values of $\bar{V}/\sigma$, the signal amplitude is well masked by the noise while the phase can still give valuable information about the signal. Since the mean value of the phase is the true value, a non-random relation between the phase in several channels is a good criterion for detection of weak signals.

(b) Accidental errors. These errors arise from unknown operator mistakes or equipment failures, and are of an intermittent but probably gross nature. An example of such an error was the mis-setting of the antennas mentioned earlier. Such an error will go undetected unless other observations of the same source reveal it. There was one time this occurred where it was later detected and the observation discarded. It is believed that there are probably not more than a couple of other chances of this particular error. Most other types of accidental errors were eliminated by various equipment and program cross checks, so that these were not a serious problem.

(c) Systematic errors. These errors are of such a nature that they repeat in exactly the same way for each observation and therefore do not decrease over several

observations. Below, several sources of this type of error are considered, together with the means used to minimize them. Estimates of their size are given.

(1) Using wrong baseline length and orientation parameters has a serious effect on the observed phases. The least-squares fit for these parameters on the initial calibration run minimized this error to less than 0.01 parts of a fringe. Since typical noise errors were about 0.04 fringes, this error was considered negligible.

(2) The flux density calibration run to determine a consistent set of flux densities resulted in an internal error of less than ±2 percent. Again this is somewhat less than the noise errors. Actually a systematic error of this nature is not so serious since almost all observations of each source were taken with the same calibrator. The only effect would be to raise or lower the whole profile.

(3) The pointing of the antennas has been achieved to an accuracy of about 1 minute of arc. The only serious effect this can have is on the flux densities from regions of the galaxy far from its center (i.e. greater than 10 minutes of arc), where the flux was corrected for the beam smoothing. This error could be as large as 10 percent for the large galaxies.

(4) Confusion of an observation due to sources near to the source of interest was of two kinds: that caused by continuum emission, and that caused by neutral hydrogen emission. The first type was virtually eliminated because of the broadband channel which gave a very accurate estimate of the continuum radiation entering the beam. The second was more serious for certain galaxies. If the radial velocity of the galaxy was near to that of hydrogen clouds in the Galaxy, the line profiles would appear superposed. In the few cases where this occurred, the position profile provided some means of distinguishing the two sources. The position corresponding to the confusing source was always quite random, probably indicating an absence of the systematic relation between velocity and position that one expects in a distant galaxy. This property served for the cases in question, so it is believed that confusion was not a serious problem.

In view of the above discussion and results, it is possible to give a rough estimate of the detection limit for the present observations. As indicated, the most serious error was that associated with the random noise of the observation. This noise was about 0.4 flux units. When the observation was calibrated, a similar noise from the calibrator increased this to a quoted error for a half-hour

observation of about 0.5 flux units. The scatter of the individual channels around the continuum flux for the galaxies having continuum emission but no detectable hydrogen indicates that this noise error is at worst an overestimation of the actual errors. It is believed that if 0.5 flux units of hydrogen emission were in at least 3 or more channels, then there would be sufficient correlation in the corresponding fluxes and phases to give a positive result. A check of this is again seen in the observations of those galaxies having continuum but no hydrogen emission. There is a definite increase in average flux level with a decrease of the phase scatter in the presence of 0.5 flux units of continuum emission.

In most cases, then, 0.5 flux units is the detection limit for neutral hydrogen radiation. For the galaxies observed more than once, the limit is reduced correspondingly.

D. Physical Processes and Model Analysis

1. Source of the Hydrogen line at 21 cm.

The association of a magnetic dipole moment with the electron and the proton, and their corresponding interaction was originally suggested by Pauli in 1924 as an explanation of the very fine or hyperfine structure in the spectrum of many atoms. This effect was calculated by Fermi, and the energy difference for the two levels was shown to correspond to a frequency of 1420.405 MHZ. When the theory was applied to the hydrogen atom in its ground state, a very narrow line at this frequency was predicted, but suggested as impossible to detect in a practical experiment because of its extremely long life time.

Then van de Hulst (1945) and Shklovsky (1949) suggested the possibility of detecting the line astronomically because of the tremendous quantities of neutral hydrogen believed to exist in interstellar space. Their prediction proved true and the line was first observed in 1951 by Ewen and Purcell (1951).

In this section the spin-spin interaction of hydrogen atom which produces the 21 cm line will be considered in some detail. First, the interaction energy function will be derived from classical electromagnetic theory and the form of the Hamiltonian operator generated, using the rules of quantum mechanics. Second, the ground-

state hydrogen atom spin wave functions will be derived that diagonalize this operator. Finally, the energy levels will be determined, together with the approximate linewidth.

(a) The Hamiltonian. We have for the interaction energy of a magnetic dipole and magnetic field:

$$U = -\underset{\sim}{\mu} \cdot \underset{\sim}{B} \tag{1}$$

where $\underset{\sim}{\mu}$ is the dipole moment. On the other hand the magnetic potential of a dipole can be expressed as:

$$\Phi_m = \frac{\mu_0}{4\pi} \left(\underset{\sim}{\mu} \cdot \nabla\left(\frac{1}{r}\right)\right) \tag{2}$$

Applying the gradient operator to the potential gives the magnetic field as:

$$\underset{\sim}{B} = -\nabla \Phi_m = -\frac{\mu_0}{4\pi} \nabla\left[\underset{\sim}{\mu} \cdot \nabla\left(\frac{1}{r}\right)\right] \tag{3}$$

Substituting this expression into the energy relation (1), we get for the interaction energy of two magnetic dipoles a distance r apart:

$$U_{12} = -\underset{\sim}{\mu}_1 \cdot \underset{\sim}{B} = -\frac{\mu_0}{4\pi} \underset{\sim}{\mu}_1 \cdot \nabla\left(\underset{\sim}{\mu}_2 \cdot \nabla\left(\frac{1}{r}\right)\right) \tag{4}$$

or performing the indicated differentiation:

$$U_{12} = \frac{\mu_0}{4\pi}\left[\frac{\underset{\sim}{\mu}_1 \cdot \underset{\sim}{\mu}_2}{r^3} - \frac{3}{r^5}(\underset{\sim}{\mu}_1 \cdot \underset{\sim}{r})(\underset{\sim}{\mu}_2 \cdot \underset{\sim}{r})\right] \tag{5}$$

This expression is valid only away from r = 0. Considerable care must be taken to obtain a correct expression for all space. Since, for the calculation of interest, only the integral of (4) times a spherically symmetric function of space is needed, we consider:

$$I = \int_V f(\underset{\sim}{r})\, \underset{\sim}{\mu}_1 \cdot \nabla\left[\underset{\sim}{\mu}_2 \cdot \nabla\left(\frac{1}{r}\right)\right] dV \tag{6}$$

where $f(\underset{\sim}{r})$ is an arbitrary but finite and spherically symmetric function of $\underset{\sim}{r}$. Because (4) diverges only at r = 0, I is approximately

$$I \simeq f(0)\, \underset{\sim}{\mu}_1 \cdot \int_{\Delta V}\left[\underset{\sim}{\mu}_2 \cdot \nabla\left(\frac{1}{r}\right)\right] dV \tag{7}$$

where ΔV is a small volume around the origin. The remaining terms of (7) have vanished because of the assumed space symmetry of $f(\underset{\sim}{r})$. Using the integral theorem:

$$\int_V \nabla\phi\, dV = \int_S \phi\, d\underset{\sim}{S}$$

where S is the surface enclosing the volume V, we get:

$$I \simeq f(0)\, \underset{\sim}{\mu}_1 \cdot \int_S \underset{\sim}{\mu}_2 \cdot \nabla\left(\frac{1}{r}\right) d\underset{\sim}{S}$$

Performing the indicated differentiation and integrating over a small spherical surface enclosing the origin easily

gives

$$I \simeq \text{CONSTANT} \times f(0)\, \underset{\sim}{\mu}_1 \cdot \underset{\sim}{\mu}_2 \tag{8}$$

This in effect says that U_{12} is in the form of a delta function near the origin. For the present purposes, then, the Hamiltonian is of the form:

$$\hat{H} = \text{CONSTANT} \times \left(\underset{\sim}{\mu}_1 \cdot \underset{\sim}{\mu}_2\, \delta(\underset{\sim}{r})\right) \tag{9}$$

or substituting the dipole moments of the electron and proton in terms of their spins:

$$\underset{\sim}{\mu}_1 = -\mu_e \underset{\sim}{S}$$

$$\underset{\sim}{\mu}_2 = \mu_p \underset{\sim}{I}$$

we have for the Hamiltonian:

$$\hat{H} = \text{CONSTANT} \times \left(\underset{\sim}{S} \cdot \underset{\sim}{I}\, \delta(\underset{\sim}{r})\right) \tag{10}$$

This form is applicable only for wave functions having spherical symmetry in space.

(b) The Wave Functions. Since essentially all of the hydrogen in interstellar space is neutral and in the ground state, only the ground state spatial wave function will be used. Its spherical symmetry implies that it is

only the spin wave functions on the $\underset{\sim}{S} \cdot \underset{\sim}{I}$ part of $\hat{H}$ that give the energy displacements. These energy levels are:

$$E = \langle S,I \mid \hat{H}_s \mid S,I \rangle \tag{11}$$

where $|S,I\rangle$ represents the possible spin wave functions, and $\hat{H}_s$ is the spin part of the Hamiltonian. Four possible base states of the spin wave function are:

$$|+,+\rangle \ , \ |+,-\rangle \ , \ |-,+\rangle \ , \ |-,-\rangle \ , \tag{12}$$

where + and - represent the two possible spin states of the electron or proton as +1/2 or -1/2. The proper linear combination of these base states must be found that will diagonalize $\hat{H}_s$. While this can be done in a straightforward fashion, a trick will simplify things. We note that since $\hat{H}_s$ is of the form:

$$\hat{H}_s = \text{CONSTANT} \times \underset{\sim}{S} \cdot \underset{\sim}{I}$$

the dot product can be written in the form:

$$\underset{\sim}{S} \cdot \underset{\sim}{I} = \tfrac{1}{2}\left(\underset{\sim}{F}^2 - \underset{\sim}{S}^2 - \underset{\sim}{I}^2\right) \tag{13}$$

where

$$\underset{\sim}{F} = \underset{\sim}{S} + \underset{\sim}{I}$$

Therefore any eigenfunction of the total spin $\underset{\sim}{F}^2$ will be an eigenfunction of $\hat{H}_s$, because $\underset{\sim}{S}^2$ and $\underset{\sim}{I}^2$ are always diagonal for combinations of the states in (12). The eigenstates of $\underset{\sim}{F}^2$ have been worked out in many quantum mechanics texts (see, for example, Merzbacher, 1961) and the results are:

$$|+,+\rangle \ , \ \frac{1}{\sqrt{2}}\left(|+,-\rangle + |-,+\rangle\right), \ |-,-\rangle \tag{14a}$$

for $F = 1$, and

$$\frac{1}{\sqrt{2}}\left(|+,-\rangle - |-,+\rangle\right) \tag{14b}$$

for $F = 0$. These four spin wave functions diagonalize the spin Hamiltonian $\hat{H}_s$.

(c) The Energy Levels and Linewidth. It is straightforward to calculate the various energy levels of (11) using the functions of (14). We have:

$$E = \text{CONSTANT} \times \begin{cases} \frac{1}{2}(0 - 3/4 - 3/4) = -3/4 & \text{IF } F=0 \\ \frac{1}{2}(2 - 3/4 - 3/4) = 1/4 & \text{IF } F=1 \end{cases} \tag{15}$$

The $F = 1$ level has three degenerate states corresponding to the functions of (14a), while the $F = 0$ level has only one corresponding to the function of (14b). The constant in (15) is evaluated by using the ground state space wave function of hydrogen:

$$\phi = \left(\frac{me^2}{4\pi\epsilon_0\hbar^2}\right)^{3/2} \frac{1}{\sqrt{\pi}} \exp\left(-\frac{r\,me^2}{4\pi\epsilon_0\hbar^2}\right) \tag{16}$$

Integrating the square of this function times $\hat{H}_S$ over all space gives for the constant:

$$\text{CONSTANT} = \frac{4}{3}\mu_e\mu_p\frac{\mu_0}{\pi}\left(\frac{me^2}{4\pi\epsilon_0\hbar^2}\right)^3$$

The difference of the two energy levels of (15) then becomes

$$\Delta E = \frac{4}{3}\mu_e\mu_p\frac{\mu_0}{\pi}\left(\frac{me^2}{4\pi\epsilon_0\hbar^2}\right)^3$$

When account is taken of the second order corrections neglected in the above calculation, this energy corresponds to a frequency of $f = 1420.406$ MHz.

The natural linewidth of the hyperfine transition can be determined from quantum mechanics applied to magnetic dipole transitions. Following the calculations

of Wild (1952), the transition probability for the 1420 MHz line is

$$A_{21} = \frac{64\pi^2}{3hc^3}\,\nu^3\,|(2|\hat{M}|1)|^2$$

where $(2|\hat{M}|1)$ is the matrix element of the magnetic moment operator $\hat{M}$ and the two states involved, and

$$|\hat{M}| = L + 2S$$

where L and S are the angular momentum and spin quantum numbers. This equation leads to a transition probability of:

$$A_{21} = 2.85 \times 10^{-15}\ \text{sec}^{-1}$$

or a natural half-width of

$$\nu_{1/2} = A_{21}/2\pi = 4.5 \times 10^{-16}\ \text{Hz}$$

For all practical purposes, this is a zero width.

The long lifetime

$$\tau_{21} = A_{21}^{-1} \simeq 3.5 \times 10^{14}\ \text{sec}$$

can, in part, be explained by its low frequency and also by the fact that the magnetic dipole transition is first order forbidden. It is only the large quantities of neutral hydrogen in interstellar space that allow the observation of the line.

2. Statistical Equilibrium

In the last section we considered the source of the 21 cm line from neutral hydrogen and saw that it is an extremely narrow feature and hence has a very long half-life. The mechanisms of excitation and conditions of equilibrium will now be considered briefly.

Detailed calculations have been carried out by several people (see for example, Shklovsky (1949), Wild (1952), Ewen and Purcell (1951), Purcell and Field (1956), and Field (1958)) on the various physical conditions that exist where the hydrogen line is generated. Their conclusions are summarized below.

There are basically two mechanisms of excitation, collisional and radiative. For the present experiment only the collisions between hydrogen atoms need be considered since these predominate in most cases by more than an order of magnitude. The collisions are of two kinds, those where the magnetic moments of the electrons interact to cause spin flip of the electron in question, and those collisions where the electric charges of the electrons interact to cause spin flip. This first process is called spin exchange and was shown by Purcell and Field (1956) to be the dominant process at work. Field (1958) has shown that the radiative mechanism also comes largely from two sources, the ab-

sorption of radio-frequency radiation, and the hydrogen atom interaction with Lyman-α light from outside sources. Again for the case of interest we need only consider the first mechanism.

If we let P_{10} be the probability per unit time for the transition $F = 1$ to $F = 0$ due to a collision, Purcell and Field (1956) have shown that the probability of the inverse process is:

$$P_{01} = 3 P_{10} \exp(-h\nu/kT_k) \tag{1}$$

where T_k is the kinetic temperature of the region. This is a result coming from the collision calculations. If we then combine this with the well known Einstein equations for transition probabilities of induced emission and absorption:

$$I(\nu) B_{10} = A_{10} \frac{\lambda^2 I(\nu)}{2h\nu}$$

$$I(\nu) B_{01} = \frac{g_1}{g_0} I(\nu) B_{10} = 3 A_{10} \frac{\lambda^2 I(\nu)}{2h\nu} \tag{2}$$

where A and B are the Einstein coefficients, $I(\nu)$ is the radiation intensity, and g is the statistical weight of each atomic state, then the equation of equilibrium easily becomes:

$$n_1\left(P_{10} + A_{10} + A_{10}\frac{\lambda^2 I(\nu)}{2h\nu}\right)$$

$$= 3n_0\left(P_{10}\exp\left(-\frac{h\nu}{kT_K}\right) + A_{10}\frac{\lambda^2 I(\nu)}{2h\nu}\right) \qquad (3)$$

where n_1 and n_o are the populations of atoms in each energy level.

The radiation intensity $I(\nu)$ can be expressed in terms of a temperature T_R by Planck's law:

$$I(\nu) = \frac{2h\nu}{\lambda^2}\left[\exp\left(\frac{h\nu}{kT_R}\right) - 1\right]^{-1} \qquad (4)$$

and it is a common practice to define a "spin temperature" T_S to specify the relative population levels of the atom:

$$\frac{n_1}{n_o} = 3\exp\left(-\frac{h\nu}{kT_S}\right) \qquad (5)$$

This expression has thermodynamic significance if the processes leading to equilibrium are thermal, for it is just an expression of a Maxwell-Boltzmann distribution.

Using Equations (3), (4) and (5) and the approximation that all the T's are much greater than $h\nu/k \simeq 0.068\ ^\circ K$, then we get:

$$T_S = \frac{Y T_K + T_R}{1 + Y} \qquad (6)$$

where Y has been defined as:

$$y = \frac{h\nu\, P_{10}}{kT_K A_{10}} \tag{7}$$

In this expression, T_s appears as a weighted average of T_R and T_k. If $y = 0$, then T_s and therefore n_1/n_0 is determined purely by T_R. When collisions become important ($y > 0$), then T_k becomes important. Field (1958) has determined the values of y for various astronomical situations and shown that for the cases of interest for the present observations $T_S \simeq T_k$. In other words, the hydrogen is in thermal equilibrium, and its radiation losses affect this equilibrium very little. In the presence of strong continuum radiation this may no longer be true, because T_R will begin to add in a significant portion. But this will only be important where one is interested in determining the hydrogen density from the line profiles, and optical depth must be considered.

T_S has been found to be on the order of 125°K for the Galaxy (Schmidt (1957)), which justified all of the above approximations.

3. Neutral hydrogen in a galaxy.

In this section, the radiative transfer equations will be formulated, and the appropriate approximations made

for the cases of interest. A basic model of a galaxy will be proposed that is sufficiently general for the present purposes.

(a) Transfer equations. In a very straightforward fashion one can deduce that, for an assembly of atoms, $I(\nu)$, the specific intensity of radiation, obeys the differential equation:

$$\frac{dI(\nu)}{ds} = \epsilon(\nu) - K(\nu) I(\nu) \tag{1}$$

where $\epsilon(\nu)$ is the volume emissivity, $K(\nu)$ is the absorption coefficient, and s is the distance along the line of sight. The equation states that the change of intensity is equal to the emission minus the absorption. Multiplying (1) by $\exp\left[-\int_0^s K(\nu)\, ds'\right]$ and integrating over the line of sight yields:

$$I(\nu) = \int_0^\infty \epsilon(\nu) \exp\left[-\int_0^s K(\nu)\, ds'\right] ds \tag{2}$$

For a general problem we must allow for the existence of continuum radiation, and therefore realize that both $\epsilon(\nu)$ and $K(\nu)$ consist of two parts, the continuum and the line:

$$\begin{aligned} \epsilon(\nu) &= \epsilon_c(\nu) + \epsilon_\ell(\nu) \\ K(\nu) &= K_c(\nu) + K_\ell(\nu) \end{aligned} \tag{3}$$

In the region of frequencies adjacent to the line, $K(\nu)$ is very small so that (2) becomes.

$$I(\nu) = \int_0^\infty \epsilon_c(\nu)\, ds \tag{4}$$

and also within the line $K_\ell(\nu) >> K_c(\nu)$ so that

$$I(\nu) = \int_0^\infty [\epsilon_c(\nu) + \epsilon_\ell(\nu)] \exp\left[-\int_0^s K_\ell(\nu) ds'\right] ds \tag{5}$$

It is common in this type of calculation to write the intensity in terms of brightness temperatures by means of Rayleigh-Jean's Law:

$$T_b(\nu) = \frac{\lambda^2 I(\nu)}{2k} \tag{6}$$

One can then express the excess brightness temperature of the line feature over the continuum brightness temperature by taking the difference between (5) and (4), using (6):

$$\Delta T_b(\nu) = \frac{\lambda^2}{2k} \int_0^\infty [\epsilon_c(\nu) + \epsilon_\ell(\nu)] \exp\left[-\int_0^s K_\ell(\nu) ds'\right] ds - \frac{\lambda^2}{2k} \int_0^\infty \epsilon_c(\nu)\, ds \tag{7}$$

If ΔT_b is positive we have an emission line while if it is negative, the line appears in absorption. Equation (7) is the 21 cm radiative transfer equation that will be used later.

(b) A model galaxy. It remains to express Equation (7) in terms of the approximate physical processes within the galaxy by defining its geometry, dynamical parameters, and the frequency dependence of its emission and absorption coefficients.

From the well known optical and radio properties of galaxies it is possible to approximate the highly flattened spiral galaxy, that is of interest to us, by a very thin rotating disc. Essentially all of the gas is confined to this disc and rotating with it. Studies of neutral hydrogen in galaxies (Epstein, 1964) indicate that it contributes only a small fraction of the mass of the galaxy, but serves as a tool to measure its rotation. Any radial component of the galaxy's systematic internal motion will be assumed small. The effect of a larger component on the line and position profiles will be determined with model analysis. Superposed on the rotation is a random velocity component arising from more or less local non-circular velocities of the hydrogen in the galaxy. This will be approximated by a gaussian distribution of velocities. The observer is considered to be very distant from the galaxy, and inclined to it. The density of hydrogen is assumed to be smooth (the effects of it being concentrated in spiral arms will be considered later) and to vary only with the distance from the center of the galaxy. While

undoubtedly the density does vary through the thickness of the disc, an average value will be assumed and considered constant. We can then write the emission and absorption coefficients at a point in the galaxy in the form:

$$\epsilon_\ell(\nu) = \epsilon_\ell \exp\left[-\left(\frac{\nu-\nu_o'}{\Delta\nu}\right)^2\right] \tag{8}$$

$$K_\ell(\nu) = K_\ell \exp\left[-\left(\frac{\nu-\nu_o'}{\Delta\nu}\right)^2\right]$$

where $\Delta\nu$ is the dispersion in frequency, due to the dispersion corresponding to the random velocity component, and ν_o' is the Doppler-shifted frequency of the line, due to rotation:

$$\nu_o' = \nu_o\left(1 - \frac{V(\varrho)\cos\phi\,\sin i}{c}\right) \tag{9}$$

where ϱ and ϕ are the cylindrical coordinates of the point ($\phi = 0$ is the major axis of the galaxy), $V(\varrho)$ is the circular velocity of the gas at that point, i is the inclination of the galaxy, and c, the velocity of light. Equation (8) can be written in this form since both coefficients are proportional to the number of atoms in a given frequency range.

We then have for the brightness temperature at

a given point in the galaxy:

$$T_b(\rho,\phi,\nu) \simeq \frac{\lambda^2}{2k}\left\{[\epsilon_\ell(\nu)+\epsilon_c(\nu)]\,\frac{[1-\exp(-K_\ell(\nu)\,t(\rho)\sec i)]}{K_\ell(\nu)}\right\} \quad (10)$$

where $t(\rho)$ is the thickness of the disc at ρ. For most of the galaxies that do contain neutral hydrogen, $\epsilon_c \ll \epsilon_\ell$, and the optical depth $\tau_\nu = K_\ell(\nu)\,t(\rho)\sec i \ll 1$, which allows us to write (10) using (9) as:

$$T_b(\rho,\phi,\nu) = \frac{\lambda^2 t(\rho)\sec i}{2k}\,\epsilon_\ell \exp\left[-\frac{\left(\nu-\nu_0+\frac{V(\rho)\cos\phi\,\sin i}{c}\right)^2}{(\Delta\nu)^2}\right] \quad (11)$$

4. The rotation curve and mass determinations.

Many approaches have been taken to relate theoretically the measured rotation curve to the mass density and total mass of the galaxy. These are reviewed and summarized by de Vaucouleurs (1959). Some of the simple models lead to nonphysical predictions when extrapolated to large radii, while the more physically real models are difficult to use for calculations. Burbidge, Burbidge, and Prendergast (1959) have developed a model of the mass distribution of highly flattened systems on the basis of

a sequence of differential spheroidal homoeoids. They have given the equation:

$$V^2(\omega) = 4\pi G(1-k^2)^{1/2} \int_0^{\omega} \frac{d(\rho)\,\rho^2\,d\rho}{(\omega^2 - k^2\rho^2)^{1/2}} \qquad (1)$$

where $V(\omega)$ is the rotational velocity as a function of a normalized distance ω from the center, $d(\rho)$ is the mass density, ρ the semimajor axis, and k is the eccentricity of the spheroids. By expanding both V^2 and d in a Taylor series, they were able to express each term in d as a function of only one term in V^2. Therefore if the measured V^2 is expanded in several terms, the corresponding mass can be calculated. Schmidt (1956) used a similar type of analysis on the Galaxy with four spheroids, but instead made approximations to the mass densities of these spheroids expanded in two terms of a Taylor series varying inversely with ρ.

The difficulty with these models is that the mass distribution predicted for either the galaxy's center or its extremities is often non-physical. Brandt (1960 a,b) has attempted to eliminate some of the problem by assuming a rotation curve of a certain form. The curve he suggests is a general form of that originally used by Lohman (1954) and has three free parameters. The curve increases in velocity like a solid body near the

center, but reaches a maximum and diminishes into a Keplerian tail for greater distances. Two free parameters give the velocity and radius of the "turnover" point (i.e. the maximum velocity of the curve, and the radius at which it occurs), and an index determines the nature of the curve around the turnover point. The curve can be written as:

$$V(\rho) = \frac{V_{To}\,(3)^{3/2n}\left(\frac{\rho}{\rho_{To}}\right)}{\left[1 + 2\left(\frac{\rho}{\rho_{To}}\right)^{n}\right]^{3/2n}} \qquad (2)$$

where V_{To} and ρ_{To} are the turnover velocity and radius. Insertion of (2) into (1), with the approximation that the system is a disc of zero thickness, allows one to invert the integral equation and express $d(\rho)$ as an integral of the rotation curve. The total mass can be written as:

$$M = \left(\frac{3}{2}\right)^{3/n} \frac{V_{To}^2\,\rho_{To}}{G} \qquad (3)$$

Brandt suggests an increase of 10 percent added to this mass to correct for the assumption of zero thickness.

While this form of the rotation curve does fit the solid body rotation and the turnover in velocity observed in many galaxies, it is not based on any physical

grounds. The only property of the curve that is intrinsically physical is its Keplerian form for large ρ, which is expected on theoretical ground, but has not been demonstrated observationally. The curve is convenient in that it has a mathematical form that allows Equation (1) to be inverted for some useful mass models giving estimates of the mass density of highly flattened systems. Care must be taken not to make predictions from the model which depend on the detailed nature of the curve. The estimates of total mass from an inversion of Equation (1) are sufficiently insensitive to the exact nature of the rotation curve, that the form given in Equation (2) is still quite useful for these estimates when the true rotation curves are known only approximately.

The nature of the present observations does not allow any detailed analysis of the rotation curve. Interpretation must be approached from the point of view of model analysis: in other words, assuming various simple galactic models, and using the parameters which best fit the observed results. It is felt that Brandt's model for the rotation curve and mass best serves this type of analysis because it has only three free parameters, and yet has the convenience of form mentioned above. The model deficiencies are of no consequence here, since it will be used only to estimate a total mass.

5. Synthetic observations of models.

(a) Interferometer response. To determine what the interferometer "sees" when pointed at a simple galaxy, we insert Equation (11) of Section D3 into the interferometer response Equation (7) of Section C1 and perform the necessary integration. This gives a visibility amplitude and phase which are dependent on frequency. Since the observations were taken through a set of frequency filters to give resolution in frequency, one must integrate this visibility function over each filter to obtain the observed results. The effect of the filters is to smooth the actual visibility function over the bandwidth of the filter. The filters are approximated by Gaussians. The final response is:

$$\hat{S}(\nu,\underset{\sim}{s}) = \frac{2k}{\sigma_f \lambda^2} \int T(\rho)\, \exp\left[- \frac{(\nu - V(\rho)\sin i \cos\phi)^2}{\sigma_r^2 + \sigma_f^2} + j\,\underset{\sim}{s}\cdot\underset{\sim}{\rho} \right] \rho\, d\rho\, d\phi \qquad (1)$$

where $\hat{S}(\nu,\underset{\sim}{s})$ is the complex flux (i.e. flux and phase) entering the filter corresponding to the Doppler velocity ν, $T(\rho)$ has been defined as:

$$T(\rho) = \frac{\lambda^2 t(\rho)\, \epsilon_\ell}{2k} \qquad (2)$$

from Equation (11) of Section D3, σ_r and σ_f are the widths of the Gaussians corresponding to the random velocity component and the filter width, respectively, and $\underset{\sim}{S}$ is a vector representing the interferometer baseline in the galaxy coordinates. The integral extends over the plane of the galaxy.

Equation (2) represents the temperature distribution of hydrogen on the plane of the model galaxy integrated over all velocities. As in Equation (11) of D3, the optical depth τ_v has been assumed small. If it is not small, then Equation (2) becomes:

$$T(\varrho) = \frac{\lambda^2}{2k} \frac{\epsilon_\ell}{K_\ell} \left[1 - \exp(-\tau_v) \right] \tag{3}$$

which is still a function of ϱ but not ϕ, for the model developed in D3, where the galaxy has been assumed to be a thin disc. For the present analysis, only the functional form of T is of interest, and not its actual value, or its relation to the actual hydrogen density, since in Equation (1) for the interferometer response it appears only as a scaling factor.

Henceforth we will work with $T(\varrho)$ as a "pseudo temperature", which may or may not represent the actual hydrogen density, but will approximate its two-dimensional spatial dependence in the plane of the galaxy.

It is $\hat{S}(\nu, \underset{\sim}{s})$ that has been measured, and it is the purpose of this section to determine the information contained therein.

(b) The information in one spacing. It is clear from Section C1 on the interferometer that, if $\hat{S}$ is measured for several values $\underset{\sim}{S}$, the interferometer spacing, then Equation (1) can be mathematically inverted to give $T(\varrho)$ for a given velocity range. If one also has measured $\hat{S}$ for several values of ν, $V(\varrho)$ can also be determined. The present observations determined $\hat{S}$ over the total range in velocity but for only a small range in $\underset{\sim}{S}$. Only one baseline length, with a few different orientations in some cases, was obtained. These data are insufficient to perform any kind of direct inversion to determine either $T(\varrho)$ or $V(\varrho)$ in general, but with certain assumptions some information about them can be deduced.

To show clearly what is being measured, consider Figure 4. Here is shown a galaxy viewed face on. The dashed lines are the equal radial velocity contours, projected onto the face of the galaxy, as seen by an observer looking at the galaxy from below, along the Y-axis. The inclination of the galaxy to the observer will only change the scaling of velocities corresponding to each contour, but not their shape or spatial scale. The upper diagram shows the contours for a solid body rotation curve of the

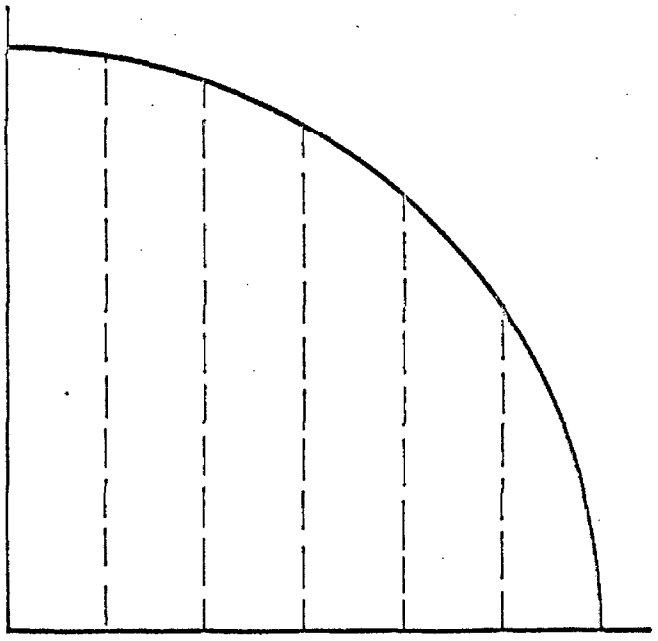

(a) SOLID BODY ROTATION

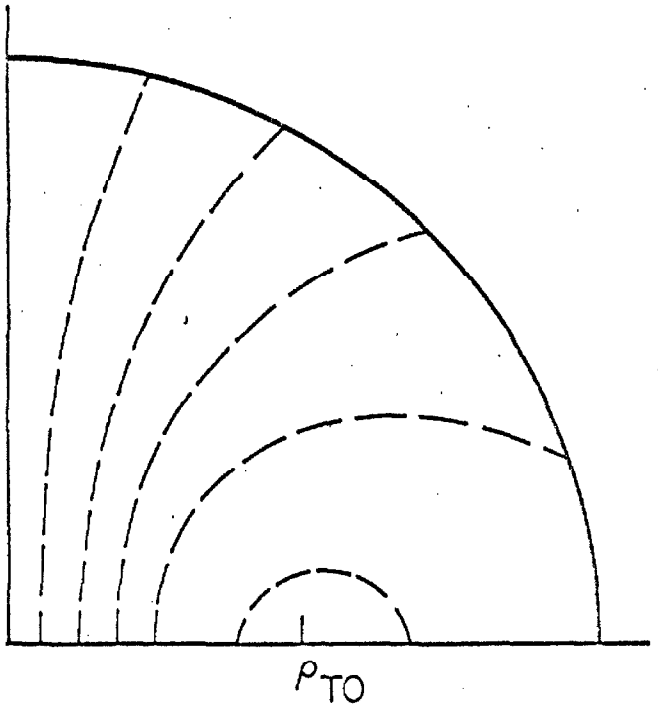

(b) NON-SOLID BODY ROTATION

Figure 4 Equi-radial-velocity contours when viewed along the Y-axis, projected onto the plane of the galaxy.

form $V(\varrho) = \text{const} \times \varrho$, and the lower diagram for the rotation curve given in the previous section, Equation (2), with $n = 3$.

For an interferometer fringe spacing fairly large compared to the galaxy, the amplitude of $\hat{S}(\omega)$ gives the total flux coming from the galaxy through the filter associated with ω (i.e. the radiation coming from between two velocity contours), and the phase of $\hat{S}(\omega)$ gives the centroid position of the flux. It is clear from Figure 4a, then, that if the galaxy moves as a solid body, $V(\varrho)$ is directly determined from the phase, and $T(\varrho)$ can be approximated from the flux if the inclination is known. On the other hand, Figure 4b shows that the centroid position of the radiation entering a given filter does not represent the ϱ for the given velocity in the rotation curve. It is always farther from the galaxy center than the corresponding ϱ, and cannot be directly related to it because of the unknown $T(\varrho)$. In this case neither $T(\varrho)$ nor $V(\varrho)$ can be determined. But if there is sufficient hydrogen at the turnover point ϱ_{TO} then the centroid of the radiation entering the filter corresponding to V_{TO}, the maximum velocity, gives an approximation to ϱ_{TO}. The smoothing due to the filters will tend to make it slightly larger than ϱ_{TO} if the turnover point is within the HI limits of the galaxy. The extent to which this is true will be

discussed below.

If one has observations at several baseline orientations, it is possible to learn something about the relative major and minor axis sizes of the hydrogen emission entering one filter. This again is plainly seen from the figure. Depending on the type of rotation curve, temperature distribution, and the inclination of the galaxy, the interferometer resolution and hence the flux entering at each velocity will vary with the angle between the projected interfometer baseline and the major axis of the galaxy. If the galaxy in question is highly inclined, one could possibly use this change in resolution with orientation to distinguish between the two types of models. Comparison of the two diagrams in Figure 4 suggests that the solid body model will always have greater resolution effects at its lower velocities as the baseline orientation changes, while the other model may reverse this, say for inclination greater than 45°.

The complex nature of Equation (1) does not allow any further general analysis. Even if $T(\varrho)$ and $V(\varrho)$ are given simple physically reasonable forms, the equation reduces to multiple integrals that cannot be evaluated in closed form. The procedure followed has been to specify the desired form of $T(\varrho)$ and $V(\varrho)$ and evaluate Equation (1) on a digital computer. This was accomplished

by dividing the galaxy into small cells and approximating the integrals by summations. In this way model line and position profiles were generated. This procedure will now be discussed in detail.

(c) Assumptions. It has been shown above that only under certain circumstances can one determine the galaxy's rotational parameters directly from the observations themselves, when only one spacing of the interferometer is used. For the sake of analysis, then, simple reasonable guesses will be made for $T(\varrho)$, and line and position profiles generated for the various reasonable types of rotation curves. The reasonableness of the assumed $T(\varrho)$ and $V(\varrho)$ will be judged on the basis of the galaxies for which these quantities are known, and also on how well they fit the observed results.

On the basis of the discussion given in Section A, the forms shown in Figure 5 will be used for $T(\varrho)$. In the figure ϱ_{HI} is the hydrogen cutoff radius (i.e. the radius at which the hydrogen density is assumed to drop to zero). From a discussion of Roberts (1966b), ϱ_{HI} seems to be about 1.5 times the optical radius of the galaxies he considers, where the optical dimensions are given by de Vaucouleurs (1964) (See Section E).

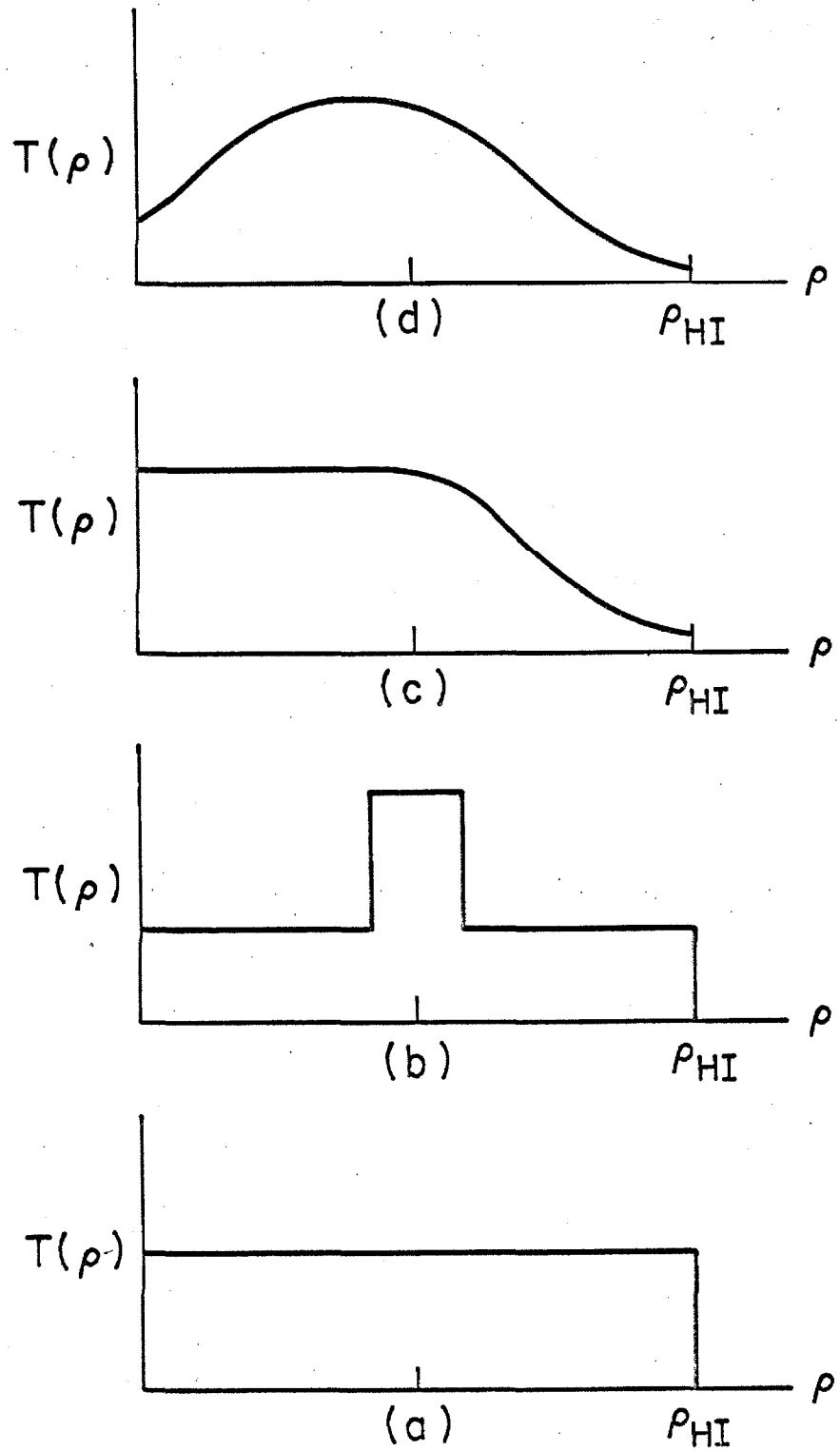

Figure 5 Model hydrogen density distributions in the plane of the galaxy.

The form of $V(\varrho)$ used will be the one discussed above that was suggested by Brandt (1960a,b). This curve, given in Equation (2) of Section D4, was used originally by Lohman (1954) on the Galaxy with $n = 3$. Roberts (1966a) has used the same curve with $n = 3/2$ to fit observations of M31. He suggests $n = 3$ also gives a good fit. For the present study $n = 3$ will be used, and the effect of a different n will be discussed. Figure 6 gives $V(\varrho)$ for $n = 1$, 3, and 10 to show the character of the curves. For the case of solid body rotation the same form for $V(\varrho)$ with $n = 3$ will be used, but ϱ_{TO} will be pushed out beyond the HI cut-off radius to give the equivalent solid body rotation curve.

(d) The model profiles and their general character. Figures 7 and 8 show what would be obtained by the interferometer when looking at the indicated model galaxies with the $T(\varrho)$ given in Figure 5c. The inclination i has been set to 90°. It should be remembered that $\sin(i)$ is basically only a scaling factor for the velocities in the model given by Equation (1). It is true that the random velocity components are not scaled by $\sin(i)$, but the effect, in this case, can clearly be seen as just a proportionately larger amount of smoothing, as shown in Figure 8 by the larger σ_R (i.e. in Figure 8, the curve for

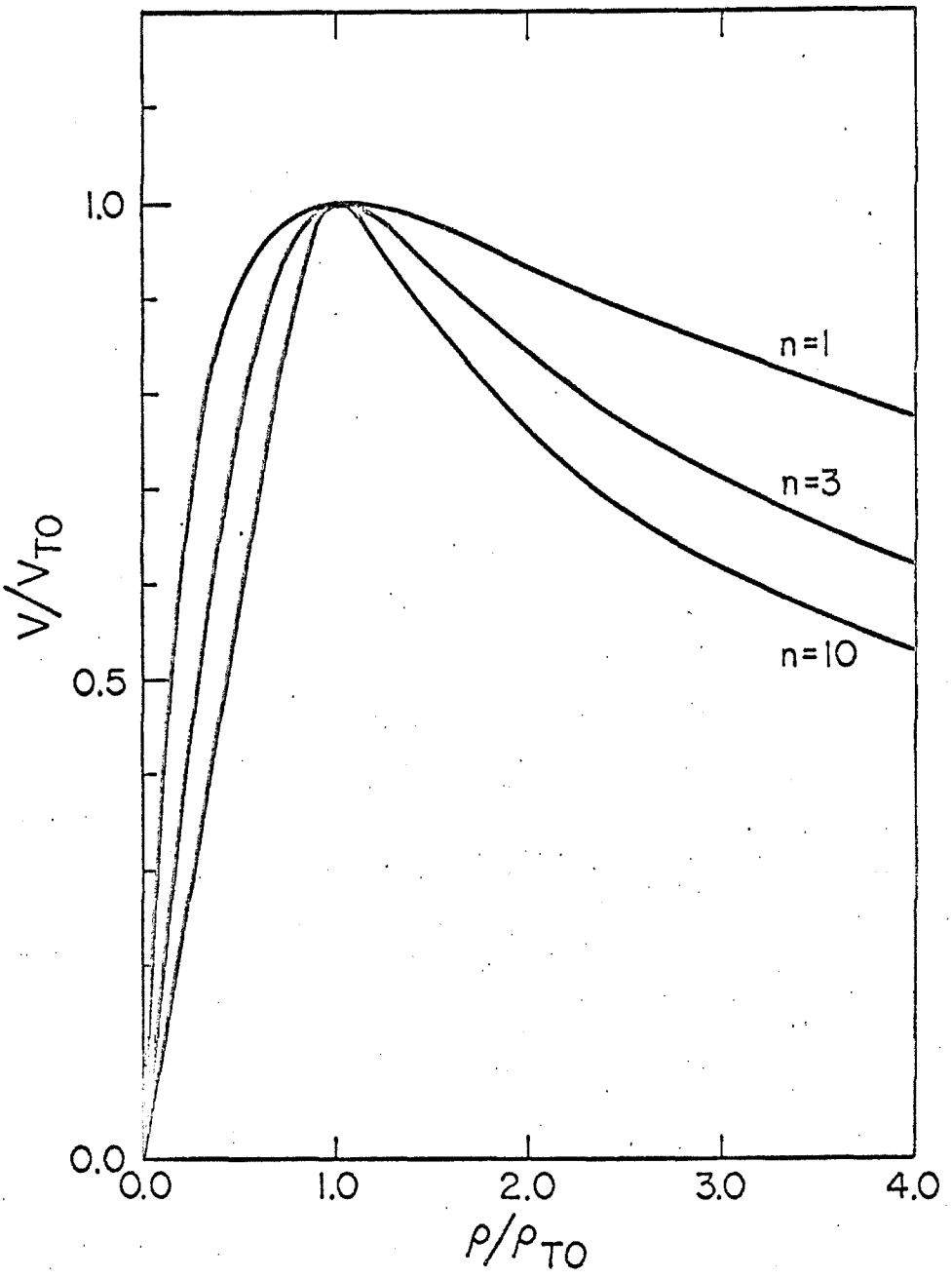

Figure 6 Model rotation curves for different n, given by Equation (2) of section D4.

$\sigma_R = 50$ with $V_{To}\sin(i) = 100$ is identical, except for scaling, to the curve one would get with $\sigma_R = 10$ and $V_{To}\sin(i) = 20$). Therefore all the general characteristics of the profiles for arbitrary i are effectively shown in the figures.

For these models, the interferometer baseline was assumed parallel to the galaxy major axis. The effects of different orientations have already been discussed some in conjunction with Figure 4. For the resolution considered, the relative amplitudes of the center and peaks of the line profiles of Figure 7 would change slightly depending on the inclination of the galaxy. There may also be an overall increase or decrease of the line profile, but the general character of the line profile will not be altered. The change in the position profile is basically, as was assumed in Section C4, just a variation in its slope proportional to the cosine of the angle between the projected baseline and the galaxy major axis.

The general character of these profiles and the effects of changing the remaining parameters in the models can be summarized as follows:

(i) Removing HI from the central regions of the galaxy, as indicated by the $T(Q)$ given in Figure 5d, lowers the center of the line profile, and lessens the slope of the position profile (i.e. at a given velocity the distance

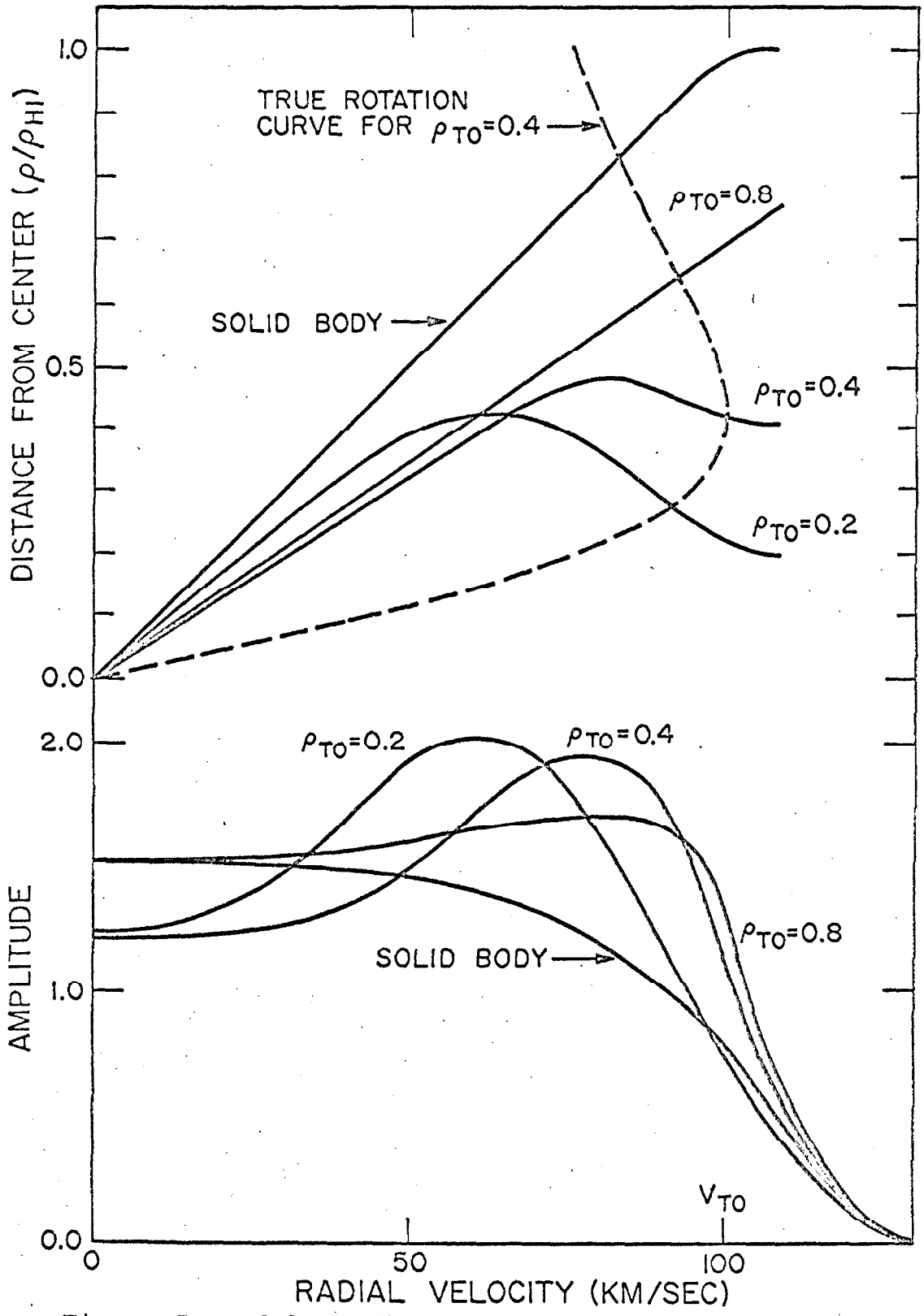

Figure 7 Model profiles for different ρ_{TO}.

becomes greater). The adding of HI to the outer regions, as shown by the $T(\varrho)$ given in Figure 5a, has almost the same overall effect as removing HI from the center. The only difference is that the turnback point in the position profile (i.e. point of maximum radius) moves out in radius. The presence of the ring structure of Figure 5b has little visible effect on either the line or position profiles. All of the above changes in $T(\varrho)$ affect the character of the profiles only slightly.

(ii) Using larger n in $V(\varrho)$ has the effect of moving the line profile peaks in toward lower velocity. Also the position profile central region becomes less steep, and its points of turnback move out in radius and lower in velocity. This turnback occurs at about the same velocity as the line profile peaks.

(iii) The presence of double peaks in the line profile indicates the existence of a velocity curve turnover well within the HI cutoff radius. Epstein (1964a) showed this was due to the larger amounts of hydrogen at the higher velocities for this type of rotation curve. It is seen clearly in Figure 4, where the area between the velocity contours roughly represents the amount of hydrogen at each velocity. As the turnover point moves outward from the galaxy center, these peaks become less prominent and merge into a single peak for solid body rotation.

(iv) The position profile obtained must be interpreted with care. Only under certain circumstances is it a good approximation to the rotation curve. As shown in Figure 7, the true rotation curve (seen for $\varrho_{To} = 0.4$ as the dotted line) is always steeper than the observed profile, the two approaching one another for the solid body case. Similar to the peak in the line profile, the turnback point in the position profile becomes less pronounced as the turnover point is moved outward from the galaxy center. It is important to note here that no reasonable $T(\varrho)$ and $V(\varrho)$ allow the movement of the double peaks of the line profile without also moving the turnback point of the position profile in the same direction. Only a change in the random velocity component will affect this relationship.

(v) Figure 8 shows the effect of different random velocity components. The tails of the line profiles are extended, and the turnback of the position profile is less pronounced when the random velocities are increased. This effectively moves the line profile peaks inward relative to the total profile width, while it moves the turnback points out, opposite to the correlation given above in (iv).

(vi) The effect of interferometer resolution is not important in the present analysis. With the assumption that the size of the region within a given velocity

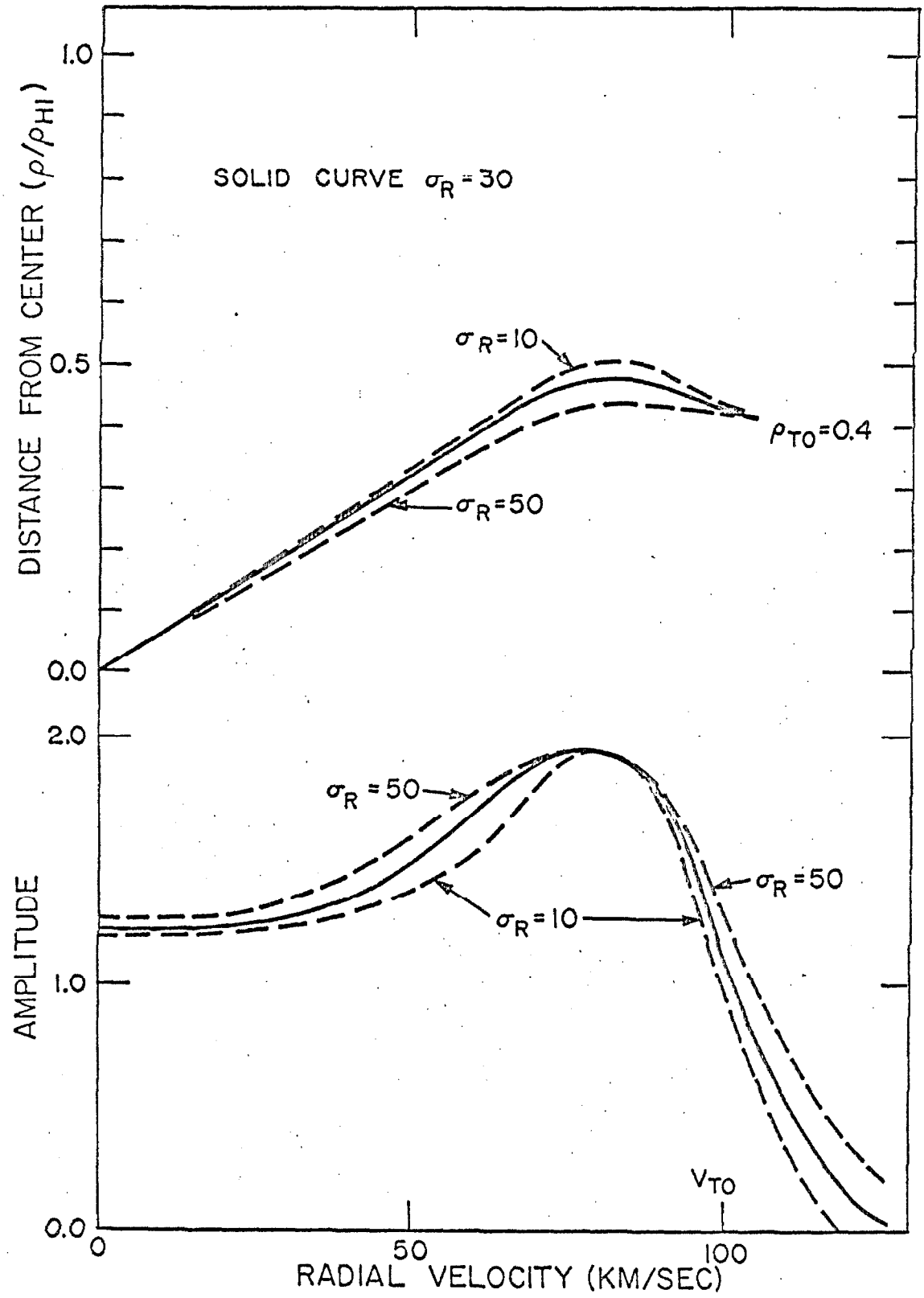

Figure 8 Model profiles for different σ_R.

interval is less than one-half the fringe spacing, there is only a general lowering of the line profile and little or no change in the position profile. For longer spacings, where the resolution does become important, the present model breaks down, and the observational results will depend critically on the detailed HI distribution instead of just on its general character. One must then consider each channel separately, and on the basis of several spacings obtain a brightness distribution for each velocity component in the usual fashion.

(vii) For observations in which noise is present, the velocity corresponding to the half-intensity level of the line profile is a fairly good estimate of the turnover velocity, and the last position in the position profile is the best estimate of the turnover radius when the line profile is double peaked. When the line profile has a single peak and no other evidence suggests non-solid body rotation within the hydrogen cutoff radius, the central slope of the position profile is best used to estimate the turnover radius.

(viii) A model including a small radial component to the normal circular velocity in the galaxy was tested and resulted in no noticeable change in the line or position profiles. The effect of this added expansion velocity is to skew the constant radial velocity contours of Figure 4 in a

counterclockwise direction around their intersection with the major axis. It would be noticeable only if the expansion velocity were comparable to the maximum radial velocity in the galaxy, and observations at several orientations of the baseline were available for intercomparison.

(ix) A model using $V(\varrho)$ = constant was also tried and resulted in profiles differing very little from those already discussed.

E. Interpretation of the Observational Results

A comparison of the observational results given in Section C4 with the model study results given in D5 suggests that the models considered are quite good in displaying the same characteristics as the actual galaxies. Since the changes in the models are so slight for the different forms of $T(\varrho)$, it is difficult to judge which is the most realistic for any given galaxy. The presence of noise in the observations, plus the likelihood that the hydrogen is not as uniformly distributed as assumed, cause irregularities in the observed profiles. These completely mask any of the subtle properties that may allow determination of the form of $T(\varrho)$. Fortunately, $T(\varrho)$ need not be known in detail to allow a reasonable estimate of the rotational characteristics to be made. The tails on a few of the line profiles suggest the possibility that the

random velocity component may be as large as 50 km/sec. The presence of noise does not make this result conclusive.

A careful comparison of the models and observational results, and use of the method given in the last section allowed an estimate to be made of the rotational parameters of most of the galaxies observed. From these the galaxy masses were calculated. These results together with other observational information are summarized in Table 5 and the notes to Table 5. In the table, column 1 contains the galaxy name, columns 2 and 3, the type and dimensions taken from de Vaucouleurs catalogue (1964), column 4, the distance of the galaxy taken from Roberts (1966b), Sersic (1960), or estimated from the radial velocity using a Hubble constant of 100 $km/sec^{-1}Mpc^{-1}$, and column 5, the inclination of the galaxy from Epstein (1964) or Danver (1942). Columns 6 through 8 contain the observational results consisting of the estimated turnover velocity and radius, and the calculated total mass of the galaxy. Finally columns 9 and 10 contain the total HI line flux, $\int \hat{S}(\nu)\, d\nu$, and the estimated mass of hydrogen. These two quantities will be discussed shortly.

The total mass was derived from the formula given in D4 Equation (3) which becomes:

$$M_T = 1.12 \times 10^5 \; V_{TO}^2 \; S \; \rho_{TO} \quad M_\odot \tag{1}$$

TABLE 5 SUMMARY OF HI RESULTS

Name NGC *IC	Type	Dimension (')	Dist. Mpc	i (°)	V_{TO} (km/s)	ρ_{TO} (')	M_T ($\times 10^{10} M_\odot$)	$\int Sdv$ (f.u.x km/s)	M_{HI} ($\times 10^9 M_\odot$)
45	Sc	8.5x 5.9	2.4	50	110	6.5	2.1	209	0.28
55	Sc	30.2x 4.9	2.4	79	87	11.0	2.2		
*10	Irr	4.0x 2.8	1.3	-	50I	5.0	$0.18I^2$	253	1.0
300	Sc	20.0x14.1	2.4	43	125	11.0	4.5		
628	Sc	9.6x 8.9	7.8	35	90	5.5	3.9	246	3.5
672	SBc	6.2x 2.3						200	
925	Sc	8.5x 4.9	6.3	53	140	3.0	4.5	239	2.2
1569	Irr	2.5x 1.2						125	
2403	Sc	15.5x 9.6	2.5	55	135	8.5	4.3		
HoII	Irr	7.4x 5.9	2.5	-	38I	3.5	$0.24I^2$	204	3.0
SexA	Irr	6.2x 5.7	1.0	-	38I	2.0	$0.30I^2$	128	0.03
*2574	Irr	12.6x 5.1	2.5	-	65I	9.0	$1.1I^2$	404	0.59
3109	Irr	14.1x 3.1	2.2	-	50I	12.0	$0.66I^2$		
3359	SBc	8.3x 2.9	11.2	(70)	133	3.5	7.7	280	8.3
3556	Sc	8.3x 2.1	10.0	84				194	4.6
4214	Irr	6.9x 5.0	3.8	-	40I	6.0	$0.40I^2$		
4236	Sc	16.6x 5.8	2.5	75	104	7.5	2.3	556	0.82
4244	Sc	15.9x 2.0	3.8	86	118	12.0	7.1	428	1.5
4258	Sb	18.6x 7.6	3.8	64					
4449	Irr	4.7x 3.0	3.8	-	65I	10.0	$1.7I^2$	353	1.2
4490	Sc	5.4x 2.7	8.0	47	110	2.5	2.7	189	2.9
4631	Sc	14.5x 2.6	8.0	84	150	7.0	14.0	570	8.6
4736	Sb	7.4x 5.9	3.8	35	280	9.0	30.0	220	0.75
5055	Sb	10.5x 5.8	8.0	59	220	5.0	22.0	316	4.8
5194	Sc	10.7x 6.9	4.6	35	157	2.5	3.2	133	0.67
5457	Sc	24.6x23.4	4.6	27	194	8.0	16.0	720	3.6
6822	Irr	16.6x12.3	0.48	-	38I	14.0	$0.11I^2$	830	0.05
6946	Sc	10.5x 9.3	3.7	31	240	8.0	19.0	546	1.8
7640	Sb	11.0x 2.2	6.4	(90)	125	7.5	8.3	266	2.6
WLM	Irr							240	

$I = (\sin i)^{-1}$

Notes to Table 5

NGC 55	Data from Seielstad and Whiteoak (1965). Good example of turnback in position profile.
IC 10	P.A. of major axis was computed from baseline P.A. of 40° and 128°. There were no obvious resolution effects. The center of position profile agrees well with Roberts (1962); however, contrary to his result, the increase in effective resolution shows rotation.
NGC 300	Data from Seielstad and Whiteoak (1965).
NGC 628	Only spiral with single peaked profile. This probably is due to small inclination. Danver (1942) puts P.A. at 0°, but slope of position profile suggests more like 90°. (P.A. = 86° and i = 36° were used.)
NGC 672	This result is probably confused by the nearby galaxy IC 1727, as suggested by the asymmetry in the position profile. No mass estimate was made.
NGC 925	Possibly some asymmetry as noted by Höglund and Roberts (1965). Also the point at -7' in position profile corresponds to separate cloud SE of galaxy described by Höglund and Roberts.
NGC 1569	No distance available. Peak at zero velocity is due to galactic radiation. Both HI and continuum radiation show resolution effects with baseline P.A.
NGC 2403	Data from Seielstad and Whiteoak (1965).
Ho II	P.A. of major axis was computed from baseline P.A. of 53° and 128°. No obvious resolution effects with baseline orientation.
Sextans A	P.A. = 90° was assumed. Q_{To} and M may be larger if this P.A. is off. To Position of continuum may indicate it is not associated with galaxy.

IC 2574	Change of position profile slope with baseline P.A. suggested 60° as good major axis P.A. Resolution of higher velocity peak with baseline P.A. indicates large sizes of HI along minor axis on this side of galaxy (~ 10').
NGC 3109	Data from Seielstad and Whiteoak (1965).
NGC 3359	Inclination of 70° was assumed. Distance obtained from redshift. The points in the position profile at +10' and -13' are similar to the one in NGC 925. They were not included in estimate of ρ_{TO}.
NGC 3556	Too much uncertainty in phases to estimate ρ_{TO}.
NGC 4214	Data from Seielstad and Whiteoak (1965).
NGC 4244	Also observed by Seielstad and Whiteoak (1965). Very good agreement of data is good test for reliability of present observations.
NGC 4258	Profiles are incomplete.
NGC 4449	All points of position profile included for estimate of ρ_{TO}. Some indication of two peaks in line profile. Very extensive wings are also exhibited in line profile, as was also found by Epstein (1964).
NGC 5194/5	Used P.A. of major axis = 42° (Danver 1942).
NGC 5457	Good example of turnback in position profile.
NGC 6822	Used same major axis P.A. as Volders and Högbom (1961).
NGC 7640	Used redshift for distance.
WLM	No distance available. Rotation may be present, and visible if observed along P.A. = 0°.

or

$$M_T = 1.94 \times 10^5 \; V_{TO}^3 \; S/A \qquad M_\odot$$

where V_{TO} is in km/sec, ρ_{TO} is in minutes of arc, S is the distance to the galaxy in Mpc, A is the central gradient of the position profile in the same units, and $M_\odot$ is the mass of the Sun. These values have been increased by 10 percent as suggested by Brandt, to allow for the finite thickness of the galaxies.

The results of the preliminary survey of Seilestad and Whiteoak (1965) have been reexamined in view of the model analysis, and new estimates made of their rotational parameters. The galaxies are NGC 55, 300, 2403, 3109, and 4214; they are also included in Table 5.

One serious source of error in the masses comes from the uncertainties in the distances used. Many of the distance estimates may easily have errors as large as 50 percent, which enter directly in the mass determination. It is difficult to give a meaningful estimate of the errors in the turnover velocities and radii for the individual galaxies because of the method used for their determination from the profiles. But it is believed that errors in these two parameters will lead to an error in the mass of not greater than about ±50 percent. The total uncertainties in the masses, then, can be as large as 100 percent.

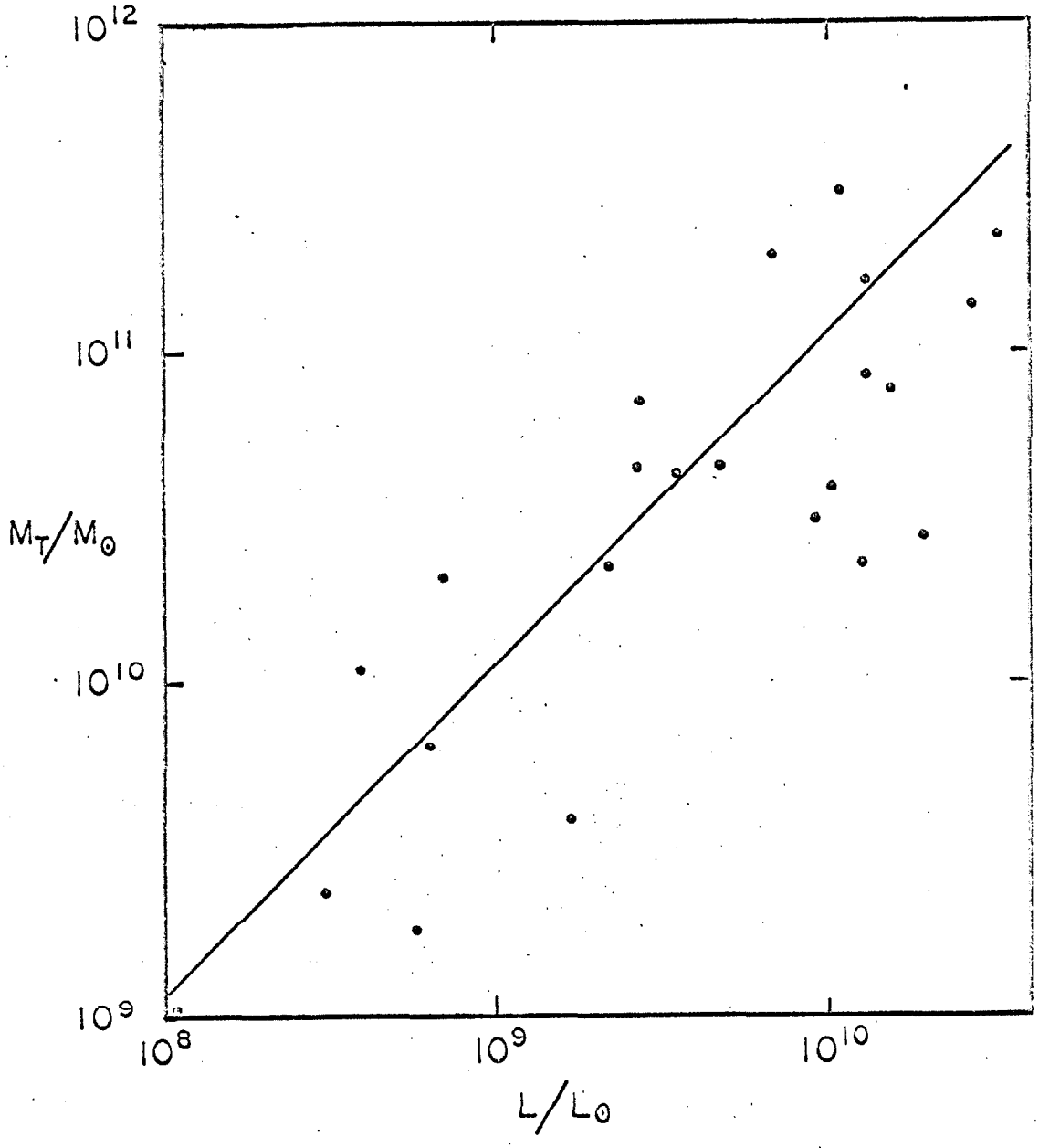

Figure 9 Plot showing the correlation of the total mass and luminosity for the detected galaxies. The solid line has slope of 11.3 .

Previous mass estimates for many of the galaxies listed here are given in Epstein (1964) and Roberts (1966b). The present results are in very good agreement in most cases. Where there is disagreement, the present results are usually larger and can be attributed to the larger turnover radius used. For the previous estimates, the turnover radius used was usually just an estimate based on the optical size of the galaxy.

Of some interest to astronomers is the relationship between the total mass M_T and the luminosity L of galaxies. Knowledge of such a relationship would allow estimates of the mass of galaxies for which the mass cannot be measured, but the luminosity can. Using luminosities from Roberts (1966b) or Holmberg (1964), a plot of the total mass versus luminosity for the detected galaxies was generated, and is displayed in Figure 9. Two irregular galaxies, Sextans A and NGC 4449, have not been included because of their very large values for M_T/L (100 and 130 respectively). It is felt they can possibly be explained by a low luminosity due to obscuration, or a wrong distance. While there is considerable scatter in the points, a definite correlation of mass and luminosity exists. The average value of the ratio M_T/L is shown by the line, and gives $M_T/L = 11.3$. This is very close to the value 12.4 given by Roberts (1966b).

Table 6 presents the average properties of the detected galaxies as a function of their type. Sextans A and NGC 4449 have also been eliminated here. These values, again, are in very good agreement with the results of Epstein (1964) and Roberts (1966b). The uncertainty in the total mass-luminosity ratios doesn't allow any conclusion about a correlation for this ratio with galaxy type.

Table 6

Average Properties of Detected Galaxies

Type	Sb	Sc	Irr
No. Detected	4	16	10
Percent detected of those looked at	17	59	77
Average M_T ($\times 10^{10}$ $M_\odot$)	20.1	6.7	1.2
Average M_T/L	13.3	11.0	10.7

The term "optical size" of a galaxy has been used previously and will be used again for comparison with the turnover radii. Since the optical light intensity emitted by a galaxy does not drop abruptly to zero at some radius, but just gradually decreases, there is some need to define what is meant by this term. There are

basically two definitions of galaxy diameter: the "brightness diameter", which refers to a given isophote of specified surface brightness (usually 25.0 mag/sec^2), or the "effective diameter", which refers to the isophote within which is emitted a fraction (usually one-half) of the total photographic luminosity of the galaxy. Both of these depend on the luminosity law of the galaxy.

The dimensions given in Table 5 are of the first type, and de Vaucouleurs (1957a) has indicated that these are about 2.5 times the corresponding effective diameters for spirals. In other words, a considerable fraction of the light is within the quoted radius. Holmberg (1958) has also used the first definition, but goes down to an isophote brightness of about 26.7 mag/sec^2 (de Vaucouleurs, 1959a).

In about half of the galaxies detected, the estimated turnover radius is within or equal to the optical radius of the galaxy as quoted from de Vaucouleurs (1964). If one uses the system of determining optical radii of Holmberg (1958), as was done in Epstein (1964) and in Seielstad and Whiteoak (1965), the optical dimensions given in Table 5 should be increased by a factor of 1.3-1.5, putting almost all turnover radii well within the optical limits of the galaxies. This conclusion is opposite to that arrived at in Seielstad and Whiteoak from the preliminary survey, where the effects of the interferometer

were not fully understood. The conclusion implies that for most of the galaxies for which hydrogen was detected, more than one-half of their mass is contained within the optical dimensions given, or more than 2/3 of the mass if the Holmberg system is used. This suggests a correlation between the mass and luminosity of a galaxy, but still puts a considerable fraction of the mass in a relatively invisible form.

A comparison of the better neutral hydrogen observations with models suggests that the hydrogen cutoff radius, ρ_{HI}, is on the order of 1.3-1.8 times the optical radius as given in the table, in agreement with Roberts (1966b). The turnover radius, ρ_{TO}, is approximately one-half of ρ_{HI} for many cases.

The correlation of probability of detection of neutral hydrogen with galaxy type is in good agreement with Epstein (1964). Seventy-seven percent of the irregulars, fifty-nine percent of Sc, and seventeen percent of Sb looked at were detected, for a total of thirty-eight percent detected. No line radiation was observed in the ellipticals that were searched. All of the irregulars detected, except the inconclusive result from WLM, were definitely rotating, but in most cases their estimated masses were lower than the rest of the galaxies. Interestingly enough, the two irregulars IC 2574 and NGC 4449, that

have higher mass, show double peaked line profiles while the rest are single peaked, suggesting that these two could possibly be obscurred spirals. Part of the mass difference may be explained by the unknown inclinations.

Estimates of the total mass of hydrogen in each galaxy by integrating the line profile and using the formula of Roberts (1966b)

$$M_{HI} = 2.36\ S^2_{MPc} \int |\hat{S}(v)|dv \times 10^5\ M_\odot \qquad (2)$$

were made, but are unreliable for the following reasons:

(a) It is evident from the results, for which several orientations of the projected interferometer baseline were available, that the galaxies were partially resolved. While the model analysis has shown that this is not serious for determining the rotational characteristics, the resolution does seriously effect the integral of the line profile. This is even true for the apparently small galaxies. Comparison of the line profiles with those from galaxies also done by Epstein (1964) shows differences of flux up to a factor of 2. The large apparent sizes of the hydrogen regions within a given velocity interval, suggested by this resolution, are probably due to large random velocity components in these galaxies. The effect of these components is to smooth the regions out over the galaxy so that their

overall size is large but the change in position of the hydrogen centroid corresponding to each filter is small.

The corrections to the line profile for these resolution effects are unknown, and therefore cannot be applied.

(b) Because the form of $T(Q)$ is not known or possible to determine from the observations, proper corrections for the beam-smoothing cannot be made. Most of the galaxies looked at have HI extending out into regions where beam-smoothing becomes important.

As suggested in Section C5, even the simple corrections to the line profiles that were made there could be in error by as much as 10 percent.

The unknown corrections indicated in (a) and (b) are added to the normal uncertainties one encounters in integrating line profiles. Comparison of the calculated HI masses with those given in Roberts (1966b) suggests that most of the present results are low by more than a factor of two.

To test for any systematic deviations that may occur in the radial velocities of galaxies as determined by optical techniques compared to the radio techniques, a correlation plot has been made of the two velocities. This is found in Figure 10. The radio velocities, V_{HI}, are from Table 3, while the optical velocities, V_{Opt}, were

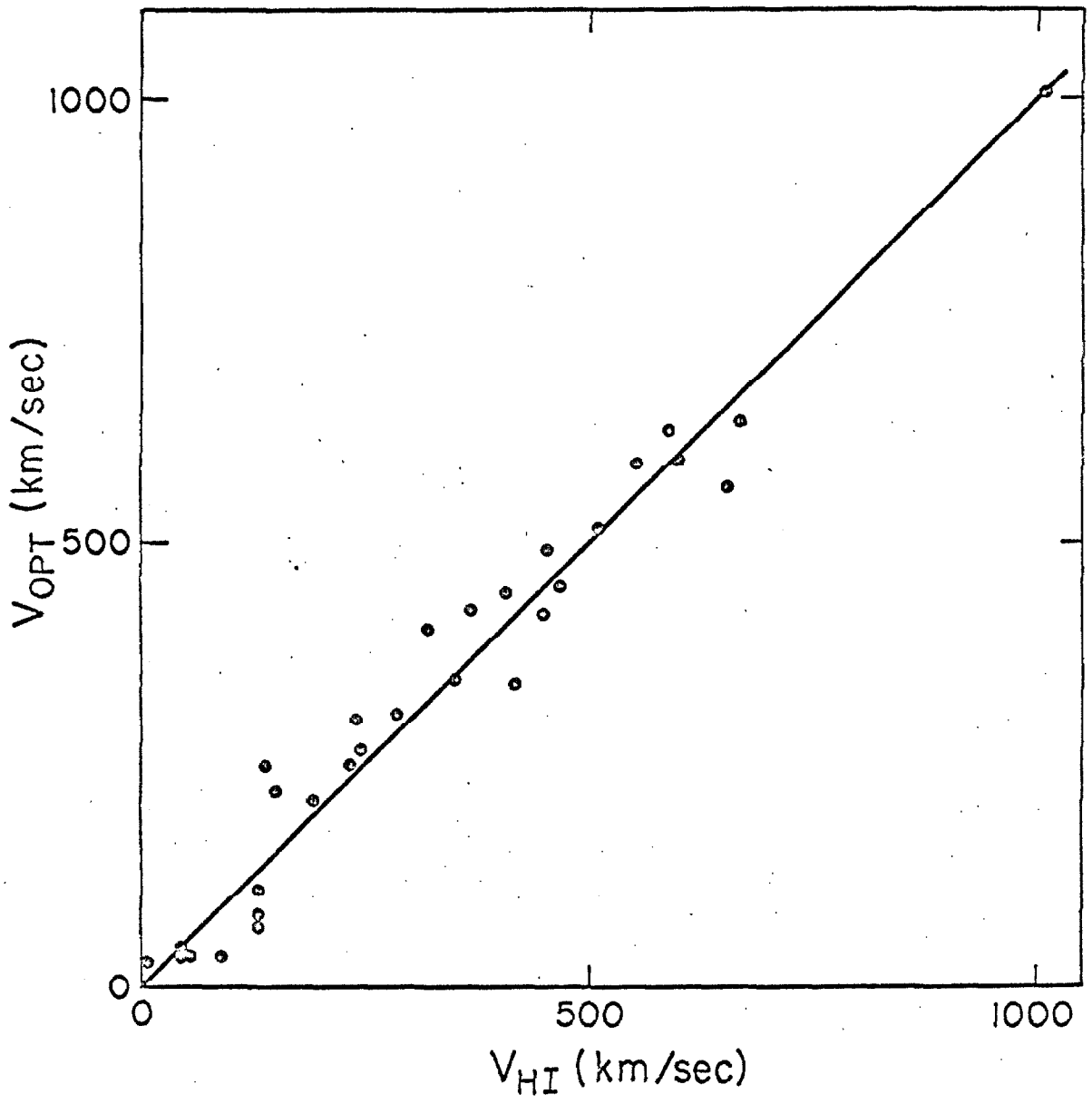

Figure 10 Plot showing the correlation of the radial velocities taken from HI and optical data.

taken from Epstein (1964) or Humason, Mayall, and Sandage (1956). The negative velocity points have been folded over into the positive range. Within the errors of the velocities, it is clear that the two techniques give the same radial velocities. This conclusion is the same as that arrived at by Roberts (1966b) after a detailed investigation of many of the same galaxies.

F. Continuum Results

A broadband continuum channel was included simultaneously with all line observations, so that the continuum emission at 21 cm was also obtained. These results are contained in Table 7. Confusion with the 90-foot antennas limits the validity of these fluxes to about 0.2 flux units. Any result less than this has not been included. The continuum of the galaxies from the preliminary survey was not measured.

The present results are in very good agreement with the continuum survey of Heeschen and Wade (1964) and Jong (1966) using the 300-foot dish at NRAO. In a few cases their results are lower, suggesting the source of emission could be approaching the size of their beam ($\sim$ 10'). If the emission region were much larger than this, the interferometer results would be lower because of resolution. Jong's results on a few galaxies give sizes much less than

TABLE 7
CONTINUUM FLUXES

Name NGC *IC	Flux	Name NGC *IC	Flux
45	0.21	4236	0.63
*10	0.75	4244	0.35
628	0.41	4258	0.88
672	0.40	4438	0.30
*1727	0.21	4449	0.40
891	0.78	4490	1.00
925	0.24	4565	0.52
1068	4.73	4594	0.21
1097	0.47	4631	1.28
1156	0.25	4736	0.42
1365	1.49	5005	0.23
1569	0.40	5055	0.50
2146	1.23	5194/5	1.53
2537	0.36	5248	0.45
Ho II	0.40	5457	0.52
2841	0.20	5866	0.33
2903	0.88	5907	0.45
3034	7.85	6015	0.44
Sex A	0.35	6217	0.27
*2574	0.47	6822	0.44
3521	0.96	6946	1.73
3556	0.34	7331	0.54
3992	0.20	7640	0.28
4214	0.28	WLM	0.57

Errors in fluxes are less than about 0.05 $\times 10^{-26}$ W $m^{-2} Hz^{-1}$.

the 10' beam.

The interferometer phases imply that for essentially all detected continuum the centroid of emission was coming from the center of the galaxy. It is felt that the low flux level, usually small region size, and central position of the emission region for the continuum justifies the assumption of little interaction of the continuum and hydrogen line emission.

G. Suggested Further Work

The present observations were performed with the idea of using a single spacing of the interferometer to measure rotation curves of galaxies. Subsequent model analysis has shown that the result obtained from the single spacing is the rotation curve only under very special circumstances, not generally met in fact. While analysis has allowed the fitting of an empirical rotation curve and estimates of masses of the galaxies detected, little information has been gained about the true rotation curves other than their general nature. One avenue of further work, then, is to perform a more complete synthesis of the galaxies with large hydrogen line signals by obtaining more interferometer spacings. Such a set of observations would give a velocity-brightness distribution and allow derivation of the detailed rotation curve in a more direct

fashion. Each velocity interval would have several interferometer spacings to determine its brightness distribution, and the combination of all velocities would determine the galaxy rotation curve. Such attempts have been made using large single dishes with beams on the order of 10' or arc, but the methods are limited to the largest of galaxies. The interferometer resolution very effectively lowers the size limit of the galaxy that can be studied, and also the resolution that can be obtained.

A further line of suggested work is a complete synthesis of the central region of the few very large galaxies. Such a program has several advantages. The larger, closer galaxies are chosen because of the stronger signal that is present, permitting more complete synthesis. Single-dish observations of these galaxies already provide the rough structure as a start, but are deficient in the central regions where the interferometer could do best. Hence, the various "pictures" would complement each other. A most important result would be the nature of the rotation curve near the center of these galaxies. The resolution that can be obtained with simple dishes is insufficient to determine whether the rotation curves in galaxies rise steeply, or gradually, to a velocity maximum. The optical evidence leaves much to be desired. The central mass density can be determined if the rotation curve is known in this region.

III. Observations of Clusters of Galaxies

A. A Search for Neutral Hydrogen in Clusters

Studies in the dynamics and stability of clusters of galaxies (see Limber, 1962) have led to the suggestion that there may be large concentrations of intergalactic gas and dust in clusters, some in the form of neutral hydrogen. This was hypothesized to explain a seeming lack of visible mass to account for cluster stability.

Working on this basis, four clusters of galaxies were searched for neutral hydrogen during the course of the observations of galaxies. The same methods of observation and reduction were used, the only difference being that four 500 kHz filters were used at 1 MHz intervals. The results are contained in Table 8.

Table 8. Fluxes from Clusters of Galaxies

Cluster	HI Flux Limit	Continuum Flux
Hercules	0.2	0.38 ± 0.04
Stephan's Q.	0.1	0.21 ± 0.03
Perseus	0.8	14.50 ± 0.10
Coma	0.2	0.58 ± 0.05

Fluxes are in units of $10^{-26}\mathrm{Wm}^{-2}\mathrm{Hz}^{-1}$

Within the limit of detection, which was at best about 0.1 flux units, no neutral hydrogen was detected. Normally this would allow one to put some sort of upper limit on the hydrogen density in the cluster, but because of the resolution effects of the interferometer, such calculations have not been attempted. The overall sizes of the HI regions that are possible, together with the change in baseline during the course of each observation would make such estimates unreliable. Further observations are suggested in part C.

B. Continuum Radiation from Clusters

In the search described in A, no neutral hydrogen signal was detected, but all four clusters exhibited continuum radiation, also seen in Table 8. This discovery led to the idea of searching many clusters of galaxies for continuum radiation. Association of radio emission with clusters had been shown before by Mills (1960), Pilkington (1964), and others, by checking the coincidence of catalogued radio positions with cluster positions or with objects within clusters, but so far no one had looked at clusters in search of radio emission.

A survey was begun with the idea of determining the fraction of clusters having radio emission, the dependence of emission probability with various cluster

parameters, and the type of object, if any, in the cluster that is associated with the radio emission. The results of the survey are presented and discussed in two papers: Rogstad, Rougoor, and Whiteoak (1965); Fomalont and Rogstad (1966).

C. Suggested Further Work

Koehler (1965) has reported finding a neutral hydrogen absorption line in 3C273 which he believes is due to intergalactic hydrogen in the Virgo cluster of galaxies. A similar feature is also reported to be visible in the radio source Virgo A (3C274) contained in the same cluster. Because the effect is extremely weak (about 0.7 percent absorption) and calibration difficult, the observations are not easy, nor the results conclusive.

A practical technique for separating the sidebands of the interferometer has been recently developed and can be used as a means of eliminating virtually all of the practical problems of such observations, so that only the random noise is the limiting factor. One possible program is to repeat Koehler's work using the above technique.

For the continuum observations, the work in clusters has suggested association of the radio emission with the brightest E type cluster members. Future work should involve surveys of the brightest E type field

galaxies, to check the statistical relation between the relative probability of radio emission in these and cluster members. Such a relation would indicate whether or not the cluster proximity affects this probability. These surveys would also serve to check the age of radio galaxies as determined by Schmidt (1966).

References

Argyle, E. 1965, Ap. J., 141, 750.

Babcock, H. W. 1939, Lick Obs. Bull, 19, 41.

Brandt, J. C. 1960a, Ap. J., 131, 293.

_____ 1960b, ibid, p. 553.

Burbidge, E. M., Burbidge, G. R., and Prendergast, K. H. 1959, Ap. J., 130, 739.

Burke, B. F. 1963, A.J. 68, 274.

Danver, C. G. 1942, Ann. Obs. Lund, No. 10, 1.

Davenport, W. B., Jr., and Root, W. L., 1958, Random Signals and Noise (McGraw-Hill), p. 145.

Dieter, N. H. 1962a, A.J., 67, 217.

_____ 1962b, ibid. 67, 313.

_____ 1962c, ibid. 67, 317.

Epstein, E. E. 1964, A.J., 69, 490.

_____ 1964a, ibid, 69, 521.

Ewen, H. I., and Purcell, E.M. 1951, Nature, 168, 356.

Field, G. B. 1958, Proc. IRE, 46, 240.

Fomalont, E. B. 1966, Ph.D. Thesis, California Institute of Technology.

Fomalont, E. B., and Rogstad, D. H. 1966, Ap.J., In Press.

Heeschen, D. S., and Wade, C. M. 1964, A.J., 69, 277.

Heidmann, J. 1961, B.A.N., XV, 314 (No. 506).

Höglund, B., and Roberts, M. S. 1965, Ap. J., 142, 1366.

Holmberg, E. 1958, Medd. Lunds Astron. Obs. Ser. II, No. 136.

_____ 1964, Arkiv. for Astr., 3, No. 30.

References, Continued

Humason, M. L., Mayall, N. U., and Sandage, A. R. 1956, A.J., 61, 97.

Jong, M. L. de. 1966, Ap. J., 144, 553.

Kellermann, K. I. 1964, A.J., 69, 285.

Kerr, F. J., Hindman, J.V., and Gum, C. S. 1959, Austr. J. Phys., 12, 270.

Kerr, F. J., Hindman, J. V., and Robinson, L. J. 1954, Austr. J. Phys., 7, 297.

Kerr, F. J., and de Vaucouleurs, G. 1955, Austr. J. Phys., 8, 508.

Koehler,J.A. 1965, private comunication.

Limber, D. N. 1962, Prob. of Extra-Galactic Research, (Macmillan Co. New York, ed. McVittie), p. 239.

Lohman, W. 1954, Zs. f. Ap., 35, 159.

Mayall, N. U., and Aller, L. H. 1942, Ap. J., 95, 5.

Mertzbacher, E. 1961, Quantum Mechanics, (John Wiley & Sons).

Mills, B. Y. 1960, Austr. J. Phys. 13, 550.

Moffet, A. T. 1962, Ap. J. Suppl, 67, 93.

Muller, C. A., and Westerhout, G. 1957, B.A.N.,, 13, 151 (No. 475).

Oort, J. H., Kerr, F. J., and Westerhout, G. 1958, M.N., 118, 379.

Pilkington, J. D. H. 1964, M.N., 128, 103.

Purcell, E. M., and Field, G. B. 1956, Ap. J., 124, 542.

Read, R. B. 1961, Trans. I.R.E., Ap-9, p. 31.

References, Continued

Roberts, M. S. 1962, A. J., 67, 437.

_____ 1966a, Ap. J., 144, 639.

_____ 1966b, Vol. IX of Stars and Stellar Systems (Univ. of Chicago Press, ed. A. and M. Sandage), Chapter 11, In Press.

Rogstad, D. H., Rougoor, G. W., and Whiteoak, J. B. 1965, Ap. J., 142, 1665.

Rougoor, G. W. 1964, B.A.N., 17, 381 (No. 6).

Rubin, V. C., Burbidge, E. M., Burbidge, G. R., Crampin, D. J., and Prendergast, K. H. 1965, Ap. J., 141, 759.

Schmidt, M. 1956, B.A.N., 13, 15 (No. 468).

_____ 1957, B.A.N., 13, 247 (No. 475).

_____ 1966, Ap. J., In Press.

Seielstad, G. A., and Whiteoak, J. B. 1965, Ap. J., 142, 616.

Sersic, J. L. 1960, Z. f. Ap., 50, 168.

Shklovsky, I. S. 1949, A. J. U.S.S.R., 26, 10.

van de Hulst, H. C. 1945, Nederlandsch. Tijdschr. v. Natuurkunde, 11, 201.

van de Hulst, H. C., Raimond, E., and van Woerden, H., 1957, B.A.N., XIV, 1 (No. 480).

van Woerden, H., Takakubo, K., and Braes, L. L. E. 1962, B.A.N., XVI, 321 (No. 524).

de Vaucouleurs, G. 1959, Encyclopedia of Physics, (Berlin: Springer-Verlag), 53, 348.

_____ 1959a, Ap. J., 130, 718.

References, Continued

de Vaucouleurs, G., and de Vaucoulers, A. 1964, Reference Catalogue of Bright Galaxies (Univ. of Texas Press).

Volders, L. 1959, B.A.N., XIV, 323 (No. 492).

Volders, L., and Hogbom, J. A. 1961, B.A.N. XV, 307 (No. 506).

Westerhout, G. 1957, B.A.N., XIII, 201 (No. 475).

Wild, J. P. 1952, Ap. J., 115, 206.